



## TEGNFORKLARING

### KVARTÆRE AVSETNINGER Quaternary deposits

1 STØRRE SAND-, GRUS- OG MORENEAVSETNINGER  
Major sand, gravel and morain deposits

### HORNEL- OG HÅSTEINSGRUPPA, MELLOMDEVONISKE AVSETNINGER Hornel and Håstein groups, middle Devonian sedimentary rocks

2 SANDSTEIN (Ålfotformasjonen)  
Sandstone (Ålfot formation)

3 KONGLOMERAT, SEDIMENTÆR BREKSJE (HAUKÅ-, OG SVARDALSFORMASJONEN)  
Conglomerate, sedimentary breccia (Haukå and Svardal formations)

4 MULIG REST AV SYENITTISK/MONZONITTISK DYPBERGART  
Possible relic of a syenitic/monzonitic intrusive rock

### SUNNARVIKGRUPPA, OMDANNA AVSETNINGSBERGARTER FRA TID Sunnarvik group, early Palaeozoic metamorphic sedimentary rocks

5 MARMOR, KALKSKIFER  
Marble, carbonate schist

6 SKIFER, METAGRÅVAKKE, FYLLONITT  
Schist, metagreywacke, phyllonite

### LYKKJEBØGRUPPA, AVSETNINGSBERGARTER OG STØRKNINGSBE Lykkjebø group, sedimentary and intrusive rocks of late Proterozoic (?) age

7 ULTRAMAFISK BERGART, SERPENTINIT  
Ultramafic rock, serpentinite

8 AMFIBOLITT  
Amphibolite

9 FYLLITTISK SKIFER, FYLLONITT  
Phyllitic schist, phyllonite

10 DOLOMITTMARMOR, KALKSKIFER  
Dolomitic marble, carbonate schist

11 GLIMMERSKIFER, FELTSPATISK GLIMMERSKIFER, GLIMMERGNEIS  
Mica schist, feldspathic mica schist, mica gneiss

12 KVARTSSKIFER, FELTSPATISK KVARTSITT, KVARTSITT OG META-ARKOSE  
Quartz schist, feldspathic quartzite, quartzite and meta-arkose

### EIKEFJORDGRUPPA, OMDANNA PREKAMBRISKE DYPBERGARTER Eikefjord group, metamorphosed Precambrian intrusive rocks

13 ULTRAMAFISK BERGART, SERPENTINIT  
Ultramafic rock, serpentinite

14 EKLOGITT, SMÅ EKLOGITTTINNESLUTNINGER (E)  
Eclogite, small eclogite bodies

15 GABBRO, MANGE STEDER OMVANDLET TIL AMFIBOLITT  
Gabbro, in many places altered to amphibolite

16 GNEISGRANITT, ØYEGRANITT  
Gneissic granite, augengranite

17 GNEIS, GNEIS MED SLIRER OG ØYNE AV FELTSPAT  
Gneiss, gneiss with veins and augens of feldspar

18 META-ANORTOSITT, STEDVIS STERK DEFORMERT OG FOLIERT  
Meta-anorthosite, in places strongly deformed and foliated

19 GNEIS, STEDVIS MED ANORTOSITT, AMFIBOLITT, GRANULITT OG ØYEGNEIS  
Gneiss, in places with anorthosite, amphibolite, granulite and augengneiss

### GRUNNFJELL, OVERVEIENDE PREKAMBRISKE BERGARTER Basement, mainly Precambrian rocks

20 GLIMMERSKIFER  
Mica schist

21 KVARTSITT  
Quartzite

22 BLASTOMYLONITTISK GNEIS  
Blastomylonitic gneiss

23 METAGABBRO, AMFIBOLITT  
Metagabbro, amphibolite

24 GRANITTISK GNEIS  
Granitic orthogneiss

25 ØYEGNEIS  
Augengneiss

26 GRANITTISK TIL GRANODIORITTISK GNEIS  
Granitic to granodioritic gneiss

27 ULTRAMAFISK BERGART  
Ultramafic rock

28 EKLOGITT  
Eclogite

29 EKLOGITT, AMFIBOLITT, METAGABBRO OG GRÅ GNEIS (KVARTSDIORITTISK?)  
Eclogite, amphibolite, metagabbro and grey gneiss (quartz-dioritic?)

### GEOLOGISKE SYMBOL Geological symbols

BERGARTSGRENSE  
Lithological contact

USIKKER BERGARTSGRENSE  
Inconformity/lithological contact

## Appendix II – Sample description

		tectonostratigraphic unit	Foliation	Lineation	Kinematic indicators	mineral content	rock texture	rock type
<b>Section AB</b>								
	18.8	basement	021/61	080/09	Layeres are folded into horizontal sub-isoclinal and isoclinal folds (10cm - 3m in length)	k-feldspar, plagioclase, bi, mu, qtz	Layered rock with mineral banding with alternating layers with higher concentrations of mica or feldspar	Granitic gneiss
							Fine-grained rock	
	18.7	basement	011/20	088/03	some prophyroclasts are flattened and sheared, k-feldspar augen with top-to west rotation, no clear folding of layers, boudinage of feldspar rich layers	k-feldspar, qtz, feldspar, bi, mu (relative high mica content)	Layered rock with mineral banding with alternating layers with higher concentrations of mica or feldspar	Mica Gneiss
							granulitic gneiss with k-feldspar augen	
	18.6	basement	018/06	102/subhoriz.	folded layers, flattened and stretched k-feldspar	60% bi, k-feldspar, qtz	foliated	feldspatic schist with k-feldspar augen
	18.5	basement	015/15	102/03	horizontal long stretched isoclinal folds (~2m long),	k-feldspar, qtz, bi, plagioclase	bi or qtz concentrated layers	granitic augengneiss
	3.3	Eikfjord nappe	352/18		brittle fractures filled with chlorite	almost 50/50 feldspar/quartz and little muscovite	foliated	Quartzofeldpatic gneiss
	3.2	Eikfjord nappe	351/18		Very fine layered rock with many little feldspar augen in a quartz matrix that are very stretched	quartz, feldspar, chlorite		Quartzofeldpatic gneiss with bi alteration to chlorite
	3.1	Eikfjord nappe	353/16		feldspar augen (2 cm), stretcht - mylonitic texture	k-feldspar, plagioclase, quartz, muscovite		Quartzofeldpatic gneiss with little mica

		tectonostratigraphic unit	Foliation	Lineation	Kinematic indicators	mineral content	rock texture	rock type
<b>Section CD</b>								
	22.1	basement			some very small folds	k-feldspar, qtz, bi	very large (5cm) k-feldspar augen feldspar rich layers and mica rich layers alternating (up to 1 m thick )	augen gneiss
	22.9	basement	342/65	263/08 (083/08)	isoclinal folding, z-fold with top to west indication varying in size assym. Folds	quartz, biotite, feldspar	banded with concentration of minerals, almost mylonitic texture, fine grained with only a few large augen giving top to west indication	Mica gneiss
	22.2	basement	353/47	75/07	horizontally shear feldspar augen 1:3 ratio very small folds	qtz,k-feldspar, plagioclase, bi	k-feldspar and plagioclase augen, finegrained matrix	augen gneiss
	22.3	basement	345/49	-		qtz,k-feldspar, plagioclase, bi	feldspar rich layered, fine grained	granitic gneiss
	22.8	on the fault	359/01	058/09	strong shearing	only feldspar, quartz, amphibole (?)	mylonitic, very fine grained (?)	
	22.7	lykkjebo group [11/green]	351/15	084/09	top to west indicating feldspar augen	mica, feldspars, qtz	fine grained matrix	mica schist with large and small k-feldspar and feldspar augen
	22.6	lykkjebo group [11/green]	347/35	276/08	feldspar augen are strongly sheared	mica, feldspars, qtz	fine grained matrix	mica schist with large and small k-feldspar and feldspar augen
	22.5	lykkjebo group [11/green]	347/70	87/08	no folds	mica's, feldspar, little qtz, garnets (0.1-0.5 cm in size)	relative large mica's and crenulated foliation around feldspar augen	mica schist with feldspar augen en garnets
	22.4	lykkjebo group [11/green]	339/21	277/04	qtz veins which are folded, irregular, fine	qtz,k-feldspar, plagioclase, mica	apparent banding	Quartzofeldpatitic gneiss

Section EF								
	22.1	basement	343/71	093/12	some very small folds	k-feldspar, qtz, bi	very large (5cm) k-feldspar augen	augen gneiss
							feldspar rich layers and mica rich layers alternating (up to 1 m thick )	
	21.6	on fault	349/68	087/horz.	non	plag, bi, chl	mylonitic texture	mylonite
	21.5	on fault	353/54	059/horz.		bi, chl, feldspar	strongly crenulated	mica schist with small feldspar augen
	21.4	nappe	351/vert.	251/14		feldspar, bi, chlorite	compositional layering strongly folded	mica gneiss
	21.3	nappe	340/71	254/03	feldspar augen indicating top to west, isoclinal folds	bi, qtz, feldspar		mica schist/gneiss with feldspar augen
	21.2	nappe	335/64	250/10	isoclinal folds	small garnets		mica gneiss with small garnets

**Appendix III** – Thin Sections

Section AB – sample 18.8



Section AB – Sample 18.7



Section AB – Sample 18.6



Section AB – Sample 18.5



Section AB – Sample 3.3



Section AB - Sample 3-1

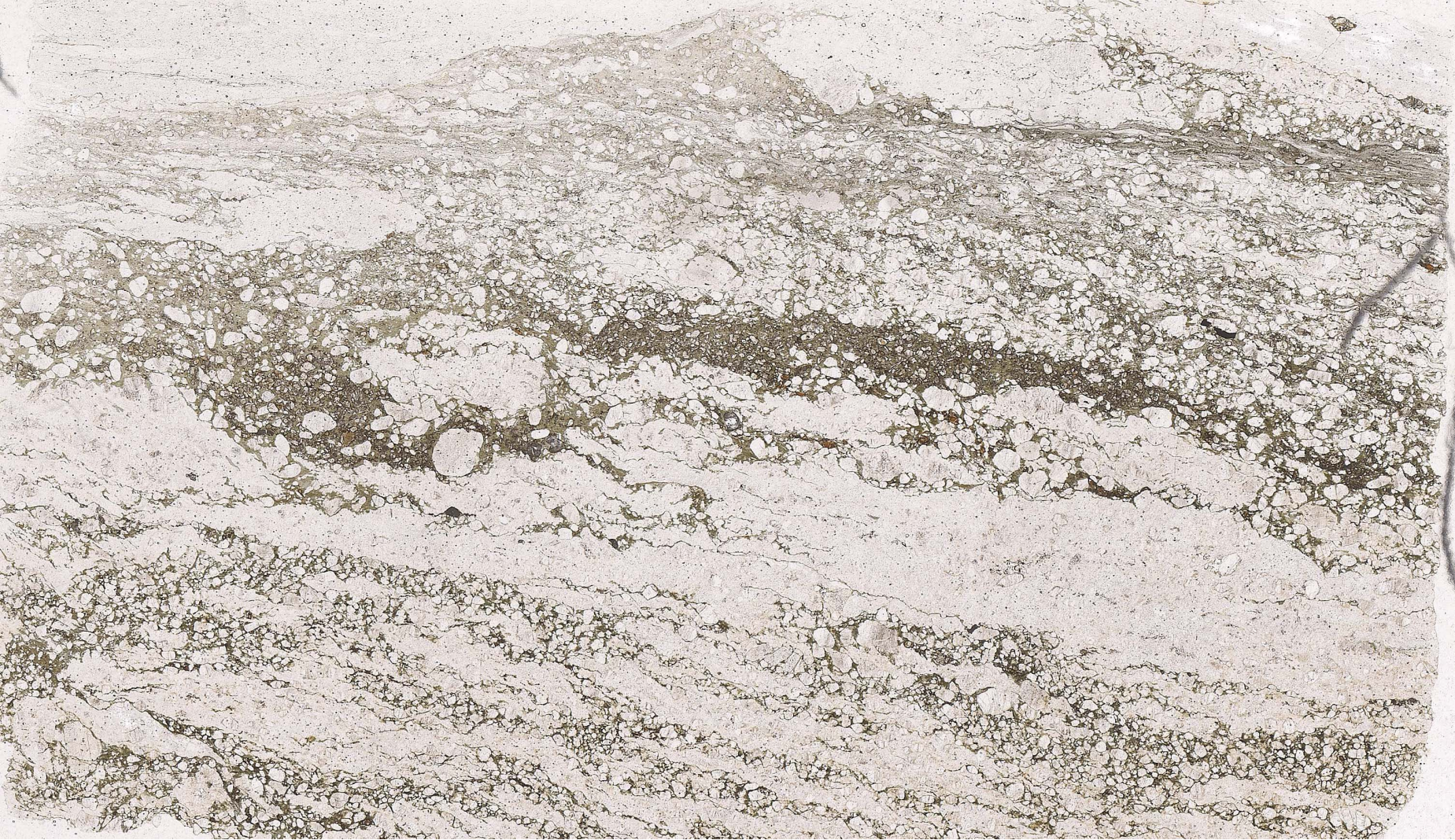


## Appendix III – Thin Sections

Section CD – sample 22.9a



Section CD - Sample 22.9b



Section CD – Sample 22.2



Section CD – Sample 22.3



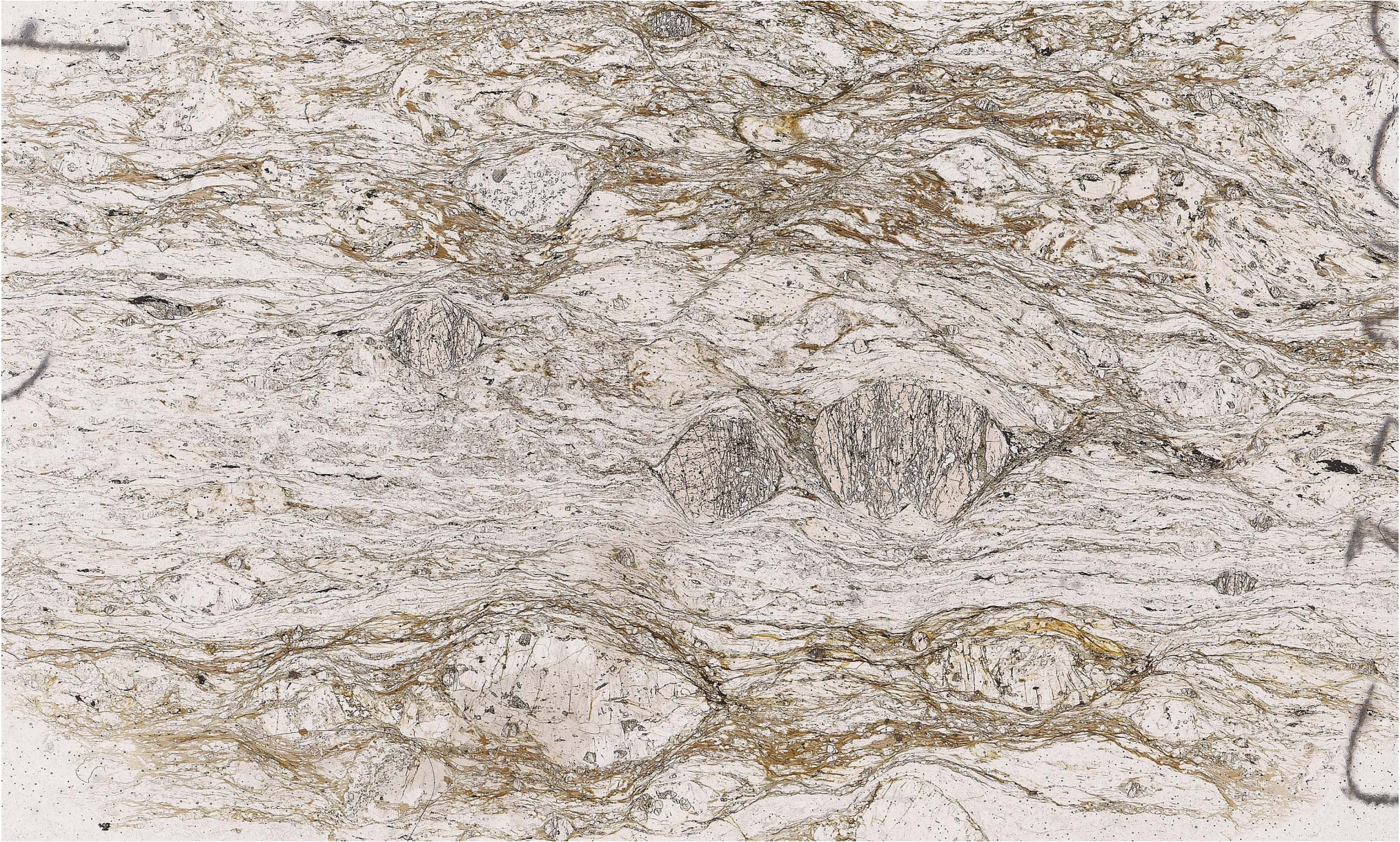
Section CD – Sample 22.7



Section CD – Sample 22.6



Section CD – Sample 22.5



Section CD – Sample 22.4



**Appendix III**

Section EF – Sample 22.1



Section EF – Sample 21.6



Section EF – 21.5



Section EF – Sample 21.4



Section EF – Sample 21.3



## Appendix IV

<b>Monazite 22.5</b>	<b>1</b>	<b>2</b>	<b>4</b>	<b>5</b>	<b>6</b>	<b>7</b>	<b>9a</b>	<b>9b</b>	<b>10</b>	<b>13</b>	<b>15</b>	<b>16</b>	<b>17</b>
<b>UO<sub>2</sub></b>	0.952	0.366	0.55	1.316	1.226	1.19	1.277	1.344	0.368	1.182	1.063	0.954	0.68
<b>PbO</b>	0.06	0.024	0.019	0.104	0.153	0.189	0.282	0.275	0.112	0.256	0.127	0.097	0.145
<b>ThO<sub>2</sub></b>	1.193	1.733	0.313	1.062	0.898	1.116	2.338	1.879	0.212	1.883	0.567	0.586	1.789
<b>P<sub>2</sub>O<sub>5</sub></b>	23.766	33.568	26.351	28.157	25.58	25.845	22.551	23.414	22.777	23.004	24.814	24.294	15.937
<b>SiO<sub>2</sub></b>	3.341	0.826	9.62	0.192	0.342	0.885	0.428	0.51	0	0.244	0.124	0.376	10.899
<b>CaO</b>	3.785	9.131	14.435	0.702	0.923	0.737	0.671	0.918	1.279	1.337	1.407	1.372	6.077
<b>S<sub>2</sub>O</b>	1.349	1.625	1.348	2.013	4.052	2.194	1.582	1.97	1.922	2.278	1.62	2.194	1.626
<b>Y<sub>2</sub>O<sub>3</sub></b>	0.462	0.183	0.026	0.03	0.174	0.163	0.112	0.089	0.422	0.1	0.2	0.033	0.029
<b>La<sub>2</sub>O<sub>3</sub></b>	7.717	8.485	5.561	8.92	8.702	9.018	8.01	8.475	9.496	8.099	9.146	9.131	5.687
<b>Ce<sub>2</sub>O<sub>3</sub></b>	23.908	23.918	18.253	29.851	27.108	30.101	27.286	29.773	29.259	29.734	30.047	30.379	19.133
<b>Pr<sub>2</sub>O<sub>3</sub></b>	3.136	3.424	2.726	4.195	3.485	4.244	3.736	4.175	3.979	4.288	4.237	4.287	2.573
<b>Nd<sub>2</sub>O<sub>3</sub></b>	9.462	11.333	8.47	13.408	11.256	12.795	12.051	12.856	12.947	13.575	13.354	13.523	8.199
<b>Sm<sub>2</sub>O<sub>3</sub></b>	1.578	1.57	1.378	2.01	1.715	1.917	1.847	1.963	2.251	1.954	2.357	2.278	1.224
<b>Eu<sub>2</sub>O<sub>3</sub></b>	0.689	0.811	0.624	1.047	0.918	1.008	0.968	1.012	1.079	0.984	1.147	1.149	0.663
<b>Gd<sub>2</sub>O<sub>3</sub></b>	0.968	0.829	0.532	0.767	0.852	0.644	0.811	0.885	1.118	0.712	1.161	1.05	0.484
<b>Dy<sub>2</sub>O<sub>3</sub></b>	0.442	0.243	0.129	0.169	0.152	0.146	0.229	0.193	0.355	0.14	0.404	0.332	0.097
<b>Total</b>	82.808	98.071	90.334	93.945	87.536	92.19	84.179	89.729	87.575	89.771	91.775	92.034	75.244
<b>U</b>	0.839	0.323	0.484	1.16	1.08	1.049	1.126	1.185	0.324	1.042	0.937	0.841	0.599
<b>Pb</b>	0.056	0.022	0.018	0.097	0.142	0.175	0.262	0.255	0.104	0.237	0.117	0.09	0.134
<b>Th</b>	1.048	1.523	0.275	0.934	0.789	0.981	2.055	1.651	0.186	1.655	0.498	0.515	1.572
<b>P</b>	10.372	14.65	11.5	12.288	11.164	11.279	9.842	10.218	9.94	10.039	10.829	10.602	6.955
<b>Si</b>	1.562	0.386	4.497	0.09	0.16	0.413	0.2	0.238	0	0.114	0.058	0.176	5.095
<b>Ca</b>	2.705	6.526	10.317	0.502	0.66	0.526	0.48	0.656	0.914	0.956	1.006	0.98	4.343
<b>S</b>	0.54	0.651	0.54	0.806	1.623	0.879	0.634	0.789	0.77	0.912	0.649	0.879	0.651
<b>Y</b>	0.364	0.144	0.02	0.024	0.137	0.128	0.088	0.07	0.332	0.079	0.157	0.026	0.023
<b>La</b>	6.581	7.235	4.742	7.606	7.42	7.69	6.83	7.226	8.097	6.906	7.798	7.786	4.849
<b>Ce</b>	20.412	20.42	15.584	25.486	23.144	25.699	23.296	25.419	24.981	25.386	25.653	25.937	16.335
<b>Pr</b>	2.68	2.926	2.329	3.585	2.978	3.626	3.192	3.567	3.4	3.664	3.621	3.663	2.199
<b>Nd</b>	8.112	9.717	7.261	11.495	9.651	10.97	10.332	11.022	11.1	11.638	11.449	11.594	7.029
<b>Sm</b>	1.361	1.354	1.189	1.734	1.479	1.653	1.593	1.693	1.941	1.685	2.033	1.964	1.056
<b>Eu</b>	0.595	0.701	0.539	0.904	0.792	0.87	0.836	0.874	0.932	0.849	0.991	0.992	0.572
<b>Gd</b>	0.84	0.719	0.462	0.665	0.739	0.558	0.704	0.768	0.97	0.618	1.007	0.911	0.42
<b>Dy</b>	0.385	0.212	0.112	0.147	0.132	0.128	0.2	0.168	0.309	0.122	0.352	0.289	0.085
<b>total REE</b>	40.966	43.284	32.218	51.622	46.335	51.194	46.983	50.737	51.73	50.868	52.904	53.136	32.545

<b>Monazite 22.5</b>	<b>18</b>	<b>19</b>	<b>21</b>	<b>22a</b>	<b>22b</b>	<b>23</b>	<b>24a</b>	<b>24b</b>	<b>24b2</b>	<b>24c</b>	<b>26</b>	<b>27e</b>	<b>27e</b>
<b>UO2</b>	0.626	0.677	0.869	1.04	1.058	2.218	0.442	0.626	0.681	0.649	0.493	0.518	0.176
<b>PbO</b>	0.1	0.125	0.111	0.077	0.103	0.284	0.022	0.071	0.066	0.059	0.051	0.05	0.065
<b>ThO2</b>	2.675	1.23	0.934	0.6	1.378	1.351	0.272	0.929	1.063	0.954	0.356	1.794	0.077
<b>P2O5</b>	14.776	17.549	23.414	22.281	26.845	19.216	28.908	25.367	25	25.877	24.14	25.984	23.622
<b>SiO2</b>	5.729	8.771	0	0	0.123	0.134	1.184	1.532	0.152	0.115	0.148	1.109	0
<b>CaO</b>	2.935	4.778	0.958	0.615	0.729	0.39	8.571	0.972	1.325	1.054	0.894	1.222	7.739
<b>S2O</b>	1.007	1.293	2.053	2.093	2.583	8.035	1.774	2.001	2.062	2	1.568	1.827	2.112
<b>Y2O3</b>	0.134	0.065	0.17	0.221	0.212	0.072	0.26	0.193	0.191	0.232	0.407	0.355	0.674
<b>La2O3</b>	4.596	5.861	8.279	8.778	8.899	6.222	7.74	9.032	9.14	9.241	9.223	8.93	7.019
<b>Ce2O3</b>	15.622	18.915	29.58	29.578	31.654	21.02	23.963	30.259	30.897	31.102	30.088	28.832	23.419
<b>Pr2O3</b>	2.193	2.577	4.098	4.272	4.45	2.928	3.335	4.1	4.592	4.198	4.409	4.032	3.41
<b>Nd2O3</b>	7.019	8.064	12.79	13.161	13.633	9.472	10.463	13.225	13.552	12.975	13.869	12.925	10.373
<b>Sm2O3</b>	1.274	1.354	1.758	2.157	1.965	1.376	1.903	2.267	2.217	2.162	2.505	2.362	1.867
<b>Eu2O3</b>	0.57	0.542	0.95	1.067	1.013	0.763	0.968	1.1	1.103	0.986	1.179	1.153	0.855
<b>Gd2O3</b>	0.662	0.548	0.965	1.087	0.664	0.717	1.062	1.091	0.966	1.019	1.27	1.286	0.902
<b>Dy2O3</b>	0.175	0.164	0.479	0.292	0.194	0.191	0.44	0.369	0.347	0.354	0.462	0.457	0.238
<b>Total</b>	60.051	72.514	87.408	87.32	95.503	74.39	91.307	93.134	93.352	92.977	91.063	92.834	82.548
<b>U</b>	0.551	0.596	0.766	0.917	0.933	1.955	0.39	0.552	0.601	0.572	0.434	0.456	0.155
<b>Pb</b>	0.093	0.116	0.103	0.072	0.95	0.264	0.021	0.066	0.061	0.054	0.048	0.046	0.067
<b>Th</b>	2.351	1.081	0.821	0.528	1.211	1.188	0.239	0.816	0.934	0.838	0.313	1.577	0.067
<b>P</b>	6.449	7.659	10.218	9.724	11.716	8.386	12.616	11.071	10.911	11.293	10.535	11.34	10.309
<b>Si</b>	2.678	4.1	0	0	0.058	0.062	0.553	0.716	0.071	0.054	0.069	0.518	0
<b>Ca</b>	2.098	3.415	0.685	0.439	0.521	0.278	6.126	0.965	0.947	0.754	0.639	0.873	5.531
<b>S</b>	0.403	0.518	0.822	0.838	1.034	3.218	0.71	0.801	0.826	0.801	0.628	0.732	0.846
<b>Y</b>	0.106	0.051	0.134	0.174	0.167	0.057	0.205	0.152	0.15	0.183	0.32	0.279	0.531
<b>La</b>	3.919	4.998	7.059	7.484	7.588	5.306	6.6	7.701	7.793	7.88	7.865	7.165	5.985
<b>Ce</b>	13.337	16.149	25.254	25.253	27.025	17.946	20.459	25.834	26.379	26.554	25.688	24.616	19.994
<b>Pr</b>	1.874	2.202	3.501	3.651	3.802	2.502	2.85	3.503	3.924	3.587	3.768	3.446	2.914
<b>Nd</b>	6.017	6.914	10.965	11.284	11.689	8.121	8.971	11.339	11.618	11.124	11.89	11.081	8.893
<b>Sm</b>	1.098	1.68	1.516	1.861	1.695	1.87	1.642	1.955	1.911	1.865	2.16	2.037	1.61
<b>Eu</b>	0.492	0.468	0.821	0.921	0.875	0.659	0.836	0.95	0.953	0.852	1.018	0.996	0.739
<b>Gd</b>	0.54	0.476	0.38	0.943	0.576	0.622	0.921	0.947	0.838	0.884	1.102	1.115	0.783
<b>Dy</b>	0.152	0.143	0.417	0.254	0.169	0.167	0.384	0.322	0.302	0.308	0.403	0.398	0.208
<b>total REE</b>	27.429	33.03	49.913	51.651	53.419	37.193	42.663	52.551	53.718	53.054	53.894	50.854	41.126

<b>Monazite 22.5</b>	<b>29a</b>	<b>29b</b>	<b>30a</b>	<b>30b</b>	<b>31</b>	<b>32</b>
<b>UO<sub>2</sub></b>	0.07	0.169	1.184	1.572	1.114	0.837
<b>PbO</b>	0.124	0.145	0.071	0.059	0.219	0.202
<b>ThO<sub>2</sub></b>	1.761	0.889	1.305	1.127	2.287	0.396
<b>P<sub>2</sub>O<sub>5</sub></b>	25.895	23.452	26.307	24.181	27.314	24.581
<b>SiO<sub>2</sub></b>	1.633	3.809	0.003	1.357	1.97	0.889
<b>CaO</b>	1.753	2.812	0.589	0.765	0.763	1.405
<b>S<sub>2</sub>O</b>	2.011	1.867	2.383	2.912	2.584	2.021
<b>Y<sub>2</sub>O<sub>3</sub></b>	0.318	0.362	0.11	0.059	0.022	0.349
<b>La<sub>2</sub>O<sub>3</sub></b>	8.98	8.194	9.035	8.351	7.821	8.893
<b>Ce<sub>2</sub>O<sub>3</sub></b>	27.56	25.082	29.731	28.393	24.75	27.769
<b>Pr<sub>2</sub>O<sub>3</sub></b>	3.971	3.411	4.146	4.015	3.515	4.032
<b>Nd<sub>2</sub>O<sub>3</sub></b>	12.377	11.197	12.759	12.443	10.607	12.138
<b>Sm<sub>2</sub>O<sub>3</sub></b>	2.404	2.047	2.037	1.975	1.632	2.15
<b>Eu<sub>2</sub>O<sub>3</sub></b>	0.964	0.974	1.002	0.97	0.811	1.052
<b>Gd<sub>2</sub>O<sub>3</sub></b>	1.021	1.248	0.947	0.81	0.698	1.106
<b>Dy<sub>2</sub>O<sub>3</sub></b>	0.409	0.375	0.269	0.196	0.195	0.347
<b>Total</b>	91.25	86.33	91.88	89.186	86.303	88.167
<b>U</b>	0.061	0.149	1.044	1.386	0.982	0.738
<b>Pb</b>	0.115	0.134	0.066	0.055	0.204	0.187
<b>Th</b>	1.548	0.781	1.147	0.99	2.01	0.348
<b>P</b>	11.301	10.235	11.481	10.553	11.92	10.728
<b>Si</b>	0.763	1.781	0.002	0.634	0.921	0.415
<b>Ca</b>	1.253	2.01	0.421	0.547	0.545	1.004
<b>S</b>	0.805	0.748	0.954	1.166	1.035	0.809
<b>Y</b>	0.25	0.285	0.087	0.046	0.017	0.275
<b>La</b>	7.657	6.987	7.704	7.12	6.669	7.583
<b>Ce</b>	23.53	21.415	25.383	24.241	21.131	23.709
<b>Pr</b>	3.393	2.915	3.542	3.431	3.004	3.445
<b>Nd</b>	10.611	9.6	10.939	10.668	9.094	10.407
<b>Sm</b>	2.073	1.765	1.757	1.704	1.407	1.854
<b>Eu</b>	0.832	0.841	0.866	0.837	0.701	0.909
<b>Gd</b>	0.886	1.083	0.822	0.703	0.606	0.96
<b>Dy</b>	0.356	0.326	0.234	0.171	0.17	0.303
<b>total REE</b>	49.338	44.932	51.247	48.875	42.782	49.17

<b>monazite 22.9</b>	<b>1b</b>	<b>2</b>	<b>3</b>	<b>7</b>	<b>8</b>	<b>9</b>	<b>10</b>	<b>11</b>	<b>12</b>	<b>13</b>	<b>14</b>	<b>15</b>
<b>UO<sub>2</sub></b>	1.184	0.22	0.258	0.217	0.23	0.958	0.11	0.191	0.004	0.16	0.208	0.689
<b>PbO</b>	0.924	1.32	1.89	1.042	1.541	1.607	0.574	0.986	0.458	0.791	0.731	0.764
<b>ThO<sub>2</sub></b>	0.323	1.054	0.092	0.013	0.111	0.051	0.002	0.052	0.095	0.035	0.016	0.071
<b>P<sub>2</sub>O<sub>5</sub></b>	18.369	22.367	24.228	22.433	20.108	24.332	12.265	29.086	18.775	26.654	27.689	22.186
<b>SiO<sub>2</sub></b>	21.404	7.129	6.617	0.996	2.974	8.573	6.607	3.305	37.323	7	7.468	13.04
<b>CaO</b>	1.806	5.567	2.997	2.685	2.878	2.703	2.393	3.664	2.496	3.251	3.466	2.703
<b>S<sub>2</sub>O</b>	0.235	0.222	0.355	0.282	0.375	0.431	0.18	0.362	0.265	0.399	0.343	0.295
<b>Y<sub>2</sub>O<sub>3</sub></b>	0.189	0.193	0.567	0.4	0.496	0.327	0.136	0.421	0	0.504	0.356	0.393
<b>La<sub>2</sub>O<sub>3</sub></b>	23.545	30.147	32.272	29.766	34.493	36.142	16.98	27.033	20.634	25.656	28.856	20.411
<b>Ce<sub>2</sub>O<sub>3</sub></b>	0.52	1.621	0.413	0.454	0.356	0.675	12.14	11.032	6.558	9.986	4.826	9.468
<b>Pr<sub>2</sub>O<sub>3</sub></b>	1.674	1.986	2.773	1.915	2.717	2.251	2.784	3.689	2.891	3.303	4.448	2.901
<b>Nd<sub>2</sub>O<sub>3</sub></b>	7.217	8.739	12.349	8.336	12.243	9.864	10.747	15.003	6.835	13.217	17.757	11.695
<b>Sm<sub>2</sub>O<sub>3</sub></b>	0.424	0.534	0.715	0.409	0.826	0.521	0.593	0.964	0.046	0.847	1.063	0.634
<b>Eu<sub>2</sub>O<sub>3</sub></b>	0.362	0.534	0.689	0.435	0.669	0.557	0.64	0.934	0.034	0.817	1.028	0.76
<b>Gd<sub>2</sub>O<sub>3</sub></b>	0.243	0.275	0.411	0.32	0.467	0.331	0.2	0.417	0	0.383	0.382	0.33
<b>Dy<sub>2</sub>O<sub>3</sub></b>	0	0.041	0.105	0.063	0.058	0.043	0.031	0.073	0	0.093	0.086	0.163
<b>Total</b>	78.419	81.954	86.431	69.767	80.54	89.365	66.381	97.213	96.413	93.097	98.723	86.503
<b>U</b>	1.044	0.196	0.228	0.191	0.203	0.845	0.097	0.168	0.003	0.141	0.183	0.608
<b>Pb</b>	0.858	1.225	1.475	0.967	1.43	1.491	0.533	0.916	0.425	0.735	0.679	0.709
<b>Th</b>	0.284	0.927	0.081	0.012	0.097	0.045	0.002	0.046	0.083	0.031	0.014	0.062
<b>P</b>	8.017	9.762	10.574	9.79	8.776	10.619	5.353	12.694	8.194	11.633	12.084	9.682
<b>Si</b>	10.005	3.332	3.093	0.466	1.39	4.007	3.088	1.545	17.446	3.272	3.491	6.096
<b>Ca</b>	1.291	3.979	2.142	1.919	2.057	1.931	1.71	2.619	1.784	2.323	2.477	1.932
<b>S</b>	0.094	0.089	0.142	0.113	0.15	0.172	0.072	0.145	0.106	0.16	0.137	0.118
<b>Y</b>	0.149	0.152	0.447	0.315	0.391	0.257	0.107	0.332	0	0.397	0.28	0.309
<b>La</b>	20.076	25.706	27.518	25.381	29.412	30.818	14.478	23.051	17.594	21.876	24.605	17.404
<b>Ce</b>	0.444	1.384	0.353	0.388	0.304	0.576	10.364	9.419	5.599	8.526	4.12	8.084
<b>Pr</b>	1.43	1.697	2.369	1.636	2.322	1.924	2.378	3.152	2.47	2.823	3.801	2.479
<b>Nd</b>	6.188	7.492	10.587	7.147	10.496	8.457	9.214	12.863	5.86	11.332	15.224	10.027
<b>Sm</b>	0.365	0.46	0.616	0.353	0.713	0.45	0.512	0.831	0.04	0.73	0.917	0.546
<b>Eu</b>	0.313	0.461	0.595	0.376	0.577	0.481	0.552	0.806	0.03	0.705	0.888	0.657
<b>Gd</b>	0.211	0.239	0.357	0.278	0.405	0.287	0.173	0.362	0	0.333	0.332	0.286
<b>Dy</b>	0	0.036	0.092	0.055	0.05	0.038	0.027	0.063	0	0.081	0.075	0.142
<b>total REE</b>	29.027	37.475	42.487	35.614	44.279	43.031	37.698	50.547	31.593	46.406	49.962	39.625

# The Nordfjord-Sogn detachment Zone in the Naustdal region, Norway

By

Caja de Vries

September, 2008  
University of Utrecht, the Netherlands

## Abstract

Late Scandian (400 – 425 Ma) exhumation in the Scandinavian Caledonides involved extensive displacement along several shear zones. The Western Gneiss Region (WGR) hosts one of these detachments also called the Nordfjord-Sogn detachment shear zone (NSDZ). It is still unclear to what extent this shear zone was involved in the exhumation of Baltica. Furthermore, whether this shear zone formed at mantle or crustal depths and how much of the displacement during exhumation was accommodated by the NSDZ. In this study these issues were addressed and researched through field research along cross-sections at several locations perpendicular to the NSDZ. Furthermore, monazite geochronology was used for determining apparent ages of monazites in the Precambrian basement and overlying nappes. As such it was possible to indentify that both the basement and nappes have been affected by the NSDZ in a up to at least 2 km wide zone which is characterized by amphibole and chlorite metamorphism. Even though the NSDZ does not runs along the basement-nappe contact continuously it is thought that because this is the only major detachment in the WGR it must have had some influence on the relative basement-nappe positioning. Monazite have an apparent age of ~ 500 Ma in both the Precambrian basement and overlying the nappe. These Finmarkian monazites implying that basement and overlying nappe went through the same metamorphic cycle in a single episode.

# Contents

## **1. Introduction**

- 1.1 The Caledonian orogeny
- 1.2 Problem statement

## **2. Geological setting**

- 2.1 The Scandinavian Caledonides
  - 2.1.1 Autochthon-Parautochthon basement
  - 2.1.2 Allochthonous nappes
  - 2.1.3 Detachment shear zone
  - 2.1.4 Devonian basin
- 2.2 The Western Gneiss Region
  - 2.2.1 The Nordfjord-Sogn Detachment zone
  - 2.2.2 Sunnfjord area

## **3. Basement-nappe contact in the Naustdal region**

- 3.1 Field method
- 3.2 Field observations
- 3.3 Petrographic analysis
- 3.4 Summary of observations at the basement-nappe contact in the Naustdal region

## **4. Monazite geochronology**

- 4.1 Introduction
- 4.2 sampling strategy
- 4.3 Analytical method
- 4.4 Age calculation technique
  - 4.4.1 Apparent age
  - 4.4.2 Isochron age
- 4.5 Results
  - 4.5.1 Samples with monazites
  - 4.5.2 WDX analysis of monazites
  - 4.5.3 Apparent age
  - 4.5.3 Isochron age

## **5. Discussion**

- 5.1 Recap of observations and results
- 5.2 Resetting of the U-Th-Pb system
- 5.3 Exhumation in the Western Gneiss Region

## **6. Conclusion**

## **7. Acknowledgements**

## **8. References**

- Appendix I. Geological map with location of the cross sections
- Appendix II. Sample description
- Appendix III. Thin sections
- Appendix IV. Table of monazite measurements

# 1. Introduction

## 1.1 The Caledonian orogeny

The Caledonides is a mountain range which formed during the Caledonian orogeny and of which at present the remnants can be found as mountain ranges along the west coast of Scandinavia, Scotland and Northern Ireland, Greenland and along the eastern coast of America and Canada. The Caledonian orogeny is marked by a sequence of tectonic events involving the closure of the Iapetus Ocean and the subsequent continent-continent collision between Baltica and Laurentia (figure 1.1). Even though the history of the Caledonides is characterized by a large number of tectonic phases, the general tectonics was that of plate convergence and subsequent extension.

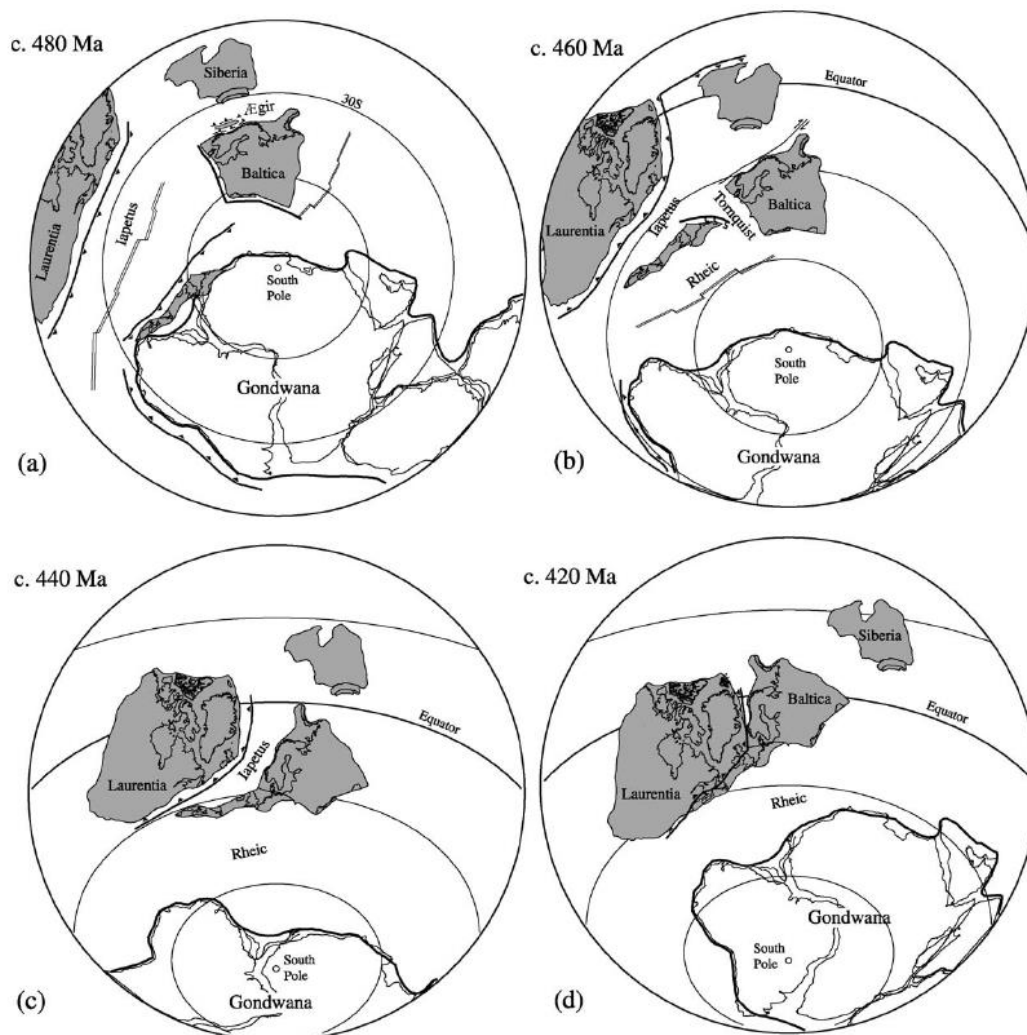


**Figure 1.1:** Reconstruction of the interaction between Baltica and Laurentia. a- b: Position of the plates at 480Ma, 460Ma, 440Ma and 420Ma. After Torsvik (1998), Torsvik et al. (1996), Cocks and Torsvik (2002) and slightly altered by Roberts (2003).

After the closure of the Iapetus Ocean sections of Baltica were forced to subduct beneath Laurentian plate. In the late Silurian and Devonian extensional movement caused the break up of Laurentia and Baltica. The two continents drifted apart and left

well exposed remnants of the Caledonides on either side of the Atlantic Ocean (Fossen and Dunlap, 1998; McKerrow et al., 2000).

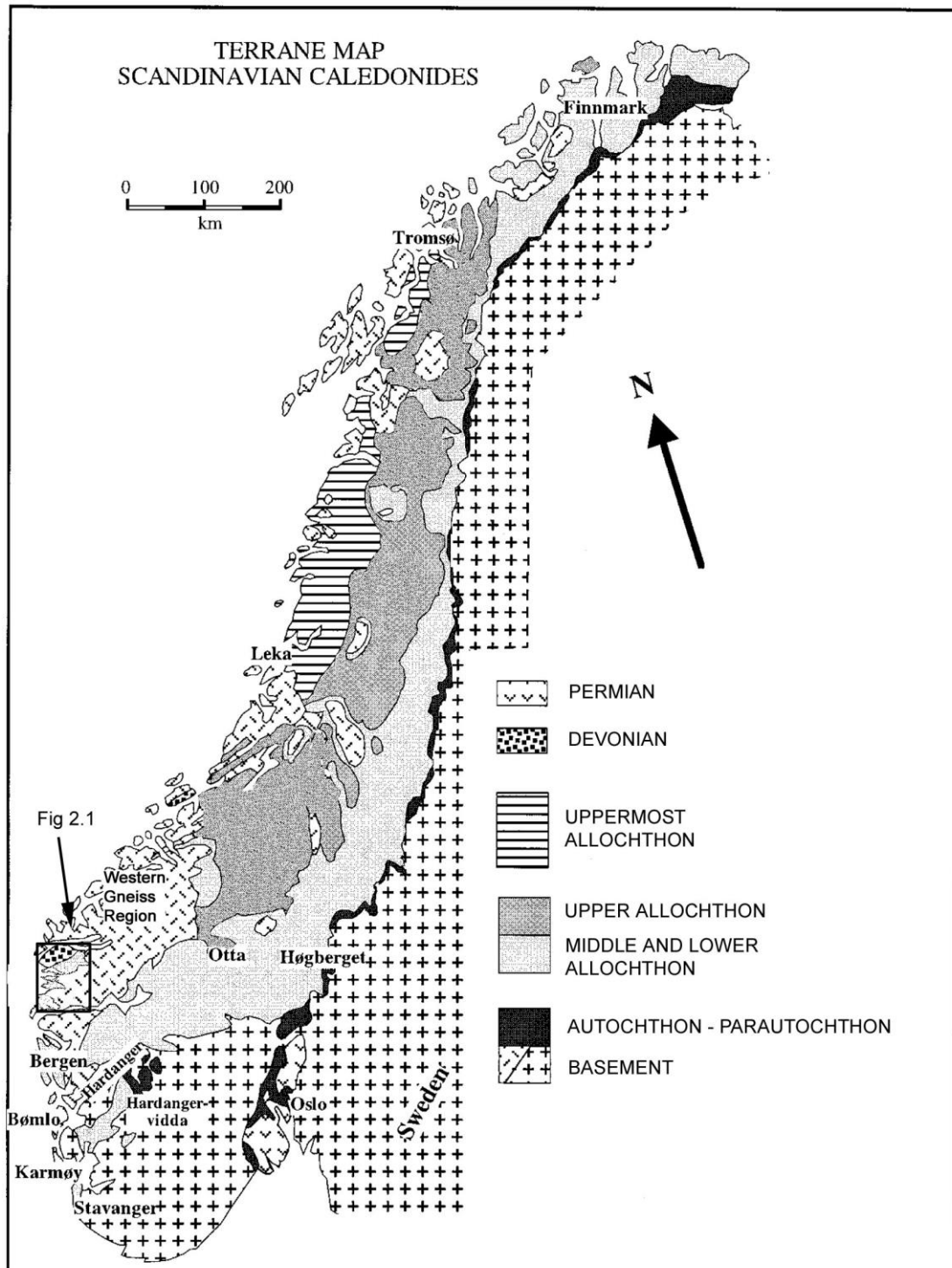


**Figure 1.2:** Schematic geological map of Scandinavia modified after Andersen (1998).

The remnants of the Caledonides on the former Western continent Baltica are called the Scandinavian Caledonides. The Scandinavian Caledonides run almost north-south through most of Norway and adjacent parts of Sweden and are about 1700 km long and 350 km wide (Hacker et al., 2003; Fossen & Dunlap, 1998).

Final assembly of the tectonostratigraphy of the Scandinavian Caledonides was established during the Scandian orogeny in the Silurian to Lower Devonian (Roberts, 2003). The Scandian orogeny is a result of the collision between Baltica and Laurentia which began at around 425 Ma whereby Baltica subducted underneath Laurentia giving rise to the characteristic distribution of the Scandinavian Caledonides in western Norway (Brueckner and Roermund, 2004). After subduction the Scandinavian Caledonides were subjected to exhumation which left a number of tectonic terrains stacked on top of each other which cover most of the Baltic Shield (Precambrian basement) (figure 1.2). Major detachment zones run through these terrains and the Precambrian basement (McKerrow et al., 2000).

The Western Gneiss Region (WGR) is a tectonic window in western Norway (figure 1.2) which surfaces the Precambrian basement of the Scandinavian Caledonides and offers an ideal opportunity to study the different tectonic units and detachments that were involved in the Scandian orogeny. The Nordfjord-Sogn Detachment is one of the largest detachments in the world and runs through the WGR along the Norwegian coast. At present, ultra-high pressure (UHP) rocks can be found locally in close relation with metamorphic lower grade rocks. Several studies found late Caledonian high pressure eclogites in the footwall of the Nordfjord-Sogn detachment surface to be within a distance of less than 3 km to the Lower to middle Devonian sedimentary rocks in the hanging wall, which have only undergone low grade metamorphism up to greenschist facies (Hacker et al., 2003). The nappes and underlying basement have been extensively stretched and thinned during large amounts of displacement and can now be found in close relation to the basement in the tectonic stratigraphy. The temporal and spatial relation between the basement and nappes is still not well understood. It is not clear how these nappes have been thinned to such a large extent and how they have been brought to so close proximity to the UHP rocks in the basement.

Various models try to explain the exhumation of the Scandinavian Caledonides and evolution of this major detachment. Firstly, models differ on what the role is of the detachment and what its formation depth is.

The single-stage exhumation model suggested by Hacker et al. (2003) sees the detachment as a single primary structure responsible for the rapid exhumation of the (U)HP rocks from the mantle into crustal levels. The detachment shear zone between these UHP rocks and the low-metamorphic rocks is thought to have initially accommodated ESE-directed nappe transport during Scandian subduction of the Baltic plate under Laurentia followed by WNW-directed ductile shearing during extensional collapse of the orogeny and bringing the (U)HP rocks in close proximity to the overlying low grade nappes (Hacker et al., 2003).

A model which separates exhumation into two episodes is the two-stage exhumation model (Andersen et al., 1994; Terry and Robinson, 2004). In this model, the detachment found at present in the WGR is believed to have accommodated the exhumation displacement at crustal depths only. Exhumation which occurred at greater depth due to gravitational collapse and orogenic extension, or imbricate thrusting and subduction channel flow is accommodated in separate structures.

The initial fast exhumation stage affected eclogites by coaxial deformation (bulk horizontal shortening and vertical stretching). The second stage at crustal levels caused vertical shortening and horizontal stretching. This stage developed at granulite to amphibolite facies and is overprinted by non-coaxial deformation that formed thick mylonites along the extensional detachments in the Scandinavian Caledonides.

There are not only numerous debates on the depth at which the detachment originated but also on the structural localization of the detachment and what role it played in stacking the different terranes at so close proximity to each other. Long sections of the detachment run along the metamorphic break between the nappe and the Precambrian basement. This has led researchers to believe that the primary detachment surface is localized at the basement-nappe contact (figure 1.3). In this model the hanging wall of the detachment consists of the different nappes stacked on top of each other. The footwall is the Precambrian basement. Significant displacement has taken place along discrete high-strain shear zones throughout the Scandinavian Caledonides. These detachments are believed to be responsible for the juxtaposition of the tectonic units (Brueckner and Van Roermund, 2004).

**Figure 1.3:** A simplified subduction and exhumation model for the Western Gneiss Region after Brueckner and Van Roermund (2004). (a) shows the collision of Baltica and Laurentia during the Scandian whereby the WGR was subducted into the mantle. (b) Post-Scandian exhumation of the WGR after slab break-off. Extensive amount of displacement is accommodated by the detachment during which stacked tectonostratigraphic units are thinned and stretched.

Others suggest that stacking of the different tectonic units was already complete before the activation of these detachments. The extensional detachment zone in the Western Gneiss Region is up to several km thick extending into the Precambrian basement (Andersen et al., 1994; Chauvet & Dallmeyer, 1992). The rocks outside this zone have not been affected by the Scandian shearing along the detachment zone. The Nordfjord-Sogn Detachment Zone (NSDZ) represents a up to 6 kilometer wide detachment zone between a brittle upper plate (hanging wall) and a ductile lower plate (footwall). This NSDZ is not limited to the basement-nappe contact and implies that the tectonostratigraphically mylonitic lower part of the nappes is situated in the footwall with the basement. In this model the upper tectonostratigraphic units (upper allochthons and Devonian sedimentary rock) were brought in close contact with the lower tectonostratigraphic units (lower allochthons and basement).

To get more insight in this problem Fossen and Dunlap (1998) looked at the extent to which the nappes and basement near the detachment shear zone had been affected by the large amounts of displacement that the nappes have undergone. Fossen & Dunlap (1998) stated that the Precambrian basement had hardly been affected by the thrusting and the detachment zone therefore is classified as thin-skinned. They believed that the detachment zone was not part of the Precambrian basement. Any Caledonian thrusting had largely been accommodated by the detachment zone but may also have been accommodated by the nappes giving a possible explanation for the extensive thinning of the nappes.

Studies done on Ar/Ar muscovite cooling ages by Chauvet & Dallmeyer (1992) and Andersen et al. (1998) complicated matters as they showed that the relationship between nappes and the underlying basement varies throughout the WGR. Chauvet & Dallmeyer (1992) tried to obtain more insight in the exhumation problem by looking at the Ar/Ar muscovite cooling ages of the basement versus cooling ages of the nappes in the WGR. They found Ar/Ar muscovite cooling ages of 399 and 403 Ma in nappes in the north of the WGR. The Precambrian basement close to these nappes gave Ar/Ar plateau ages of 393 Ma. In this area there appears to be no difference in cooling ages between the basement and the nappes. However, further to the south, nappes have cooling ages between 446 Ma and 449 Ma (Andersen et al., 1998). The basement in this area gives cooling ages of 395 Ma and 399 Ma showing a “cooling age gap” between the nappes and basement of around 50 Ma.

The purpose of this study is to find supporting field evidence for one of these models and get a better understanding of the role the NSDZ played in the exhumation of the associated tectonic units within the Scandinavian Caledonides.

## 1.2 Problem Statement

To understand the processes behind the formation of Scandinavian Caledonides it is of vital importance that individual orogenic events within the Scandinavian Caledonian orogeny are well interpreted. Many of these events can only be recognized at local scale or only in parts of the Scandinavian Caledonides, but when all are taken into account they can give important clues on the evolution of the Scandinavian Caledonides and the processes involved.

A large part of the Precambrian basement is exposed in the Western Gneiss Region in some places covered by nappes which are infolded in the basement as well as being situated around the Precambrian basement. A characteristic in the WGR is the extensive Nordfjord-Sogn detachment which is key in giving insight into the exhumation process in the Scandinavian Caledonides. One of the unsolved problems in the WGR is the short transition between the allochthon to the basement which is strongly linked to the Post-Scandian exhumation process in this region.

Further problems include: did the nappes moved separately from each other and the basement or did they all move together during exhumation? Also, to what extent are the basement and/or nappes affected by the detachment zone? Investigating these problems will increase our understanding of the exhumation process which gave shape to the Scandinavian Caledonides as we know them today.

In the following study it is tried to get a better understanding of the exhumation and processes involved.

## 2. Geological setting

### 2.1 The Scandinavian Caledonides

HP/UHP eclogite found in the Scandinavian Caledonides give rise to at least four individual tectonic events prior and during the formation of the Scandinavian Caledonides. The Finnmarkian orogeny is the youngest event which occurred during the Cambrian at around 500 Ma. The Scandian orogeny is marked by the closure of the Iapetus Ocean and collision between the two continents Laurentia and Baltica between 430 – 400 Ma. Two other simultaneous events have been recorded in the Seve Nappe Complex in Jamtland and in eclogite of the Toms Region which have been dated to be ~ 454 Ma.

High pressure minerals give evidence that Precambrian gneisses and other terrains of Baltica have been to depths of 180-200 km and underwent (U)HP metamorphism during subduction (Roermund, 2007).

At the same time, Proterozoic and lower Paleozoic metasedimentary and metavolcanic rocks and possibly basement were thrust several 100 km eastwards over the Fennoscandian Shield in a number of large thrust sheets known as nappes. The nappes have mostly a Vendian to Ordovician age (650-425/420 Myr) and are at present separated from the Precambrian basement by major detachment zones. These detachment zones are believed to have acted as thrust zones during continent-continent collision during which most of the displacement took place.

Most of the Precambrian basement is covered by these large thrust sheets and other units which are mostly metasediments. The Western Gneiss Region (WGR) on the west coast of Norway is one of the places where the Baltic Precambrian basement is exposed. This tectonic window is bordered by nappes and Devonian sediments. The protoliths of the Western Gneiss Complex (WGC) are dominated by Middle-Late Proterozoic (950-1800 Ma) rocks (Andersen and Austrheim, 2003). The Proterozoic basement is found to have experienced late Scandian ((ultra-)high pressure/ (U)HP) metamorphism during which eclogites formed. At a later stage, the basement has been partly overprinted by amphibolite facies assemblages (Griffin et al., 1985; Osmundsen & Andersen, 2001). The basement is structurally overlain by Caledonian thrust nappes which are separated by major detachment zones. These nappes can be subdivided in a lower, middle, upper and uppermost allochthon. The nappes occur both around the WGR as well as being deeply infolded in narrow Late Scandian complex synclines mostly situated along the coastal area. The nappes have undergone extreme tectonic thinning and complex ductile deformation, followed by development of mylonites, ultramylonites, and brittle faults associated with later phases of tectonic exhumation (Terry et al., 2000). This tectonic exhumation of basement and nappes to upper crustal levels was completed by c. 403 Ma (Hacker et al., 2003).

One of the largest nappes on the Scandinavian shield is the Jotun nappe in central-south Norway. It is separated from the basement by a detachment shear zone called the Hardangerfjord shear zone (Fossen , 1992). WGC basement rocks bordering the Jotun nappe are strongly affected by the late Scandian extensional deformation in a zone down to a few hundred metres below

the basement-cover contact. Towards the detachment which separates the Jotun nappe from the underlying basement the extensional fabrics become increasingly abundant and intense (Andersen, 1998).

Along the Nordfjord-Sogn Detachment zone (NSDZ) in the more Western part of the WGR, similar deformation fabrics are expected (figure 2.1). The NSDZ is a low-angle fault with normal, top to the west displacement (Brueckner & van Roermund, 2004). Together with an array of smaller normal faults and extensional detachments, this extensive shear zone produced a large amount of tectonic exhumation, bringing near ultrahigh- pressure rocks to the surface and within circa 3 km vertical distance from the low-grade Devonian conglomerate situated at the top of the tectonic stratigraphy (Hacker et al. 2003).

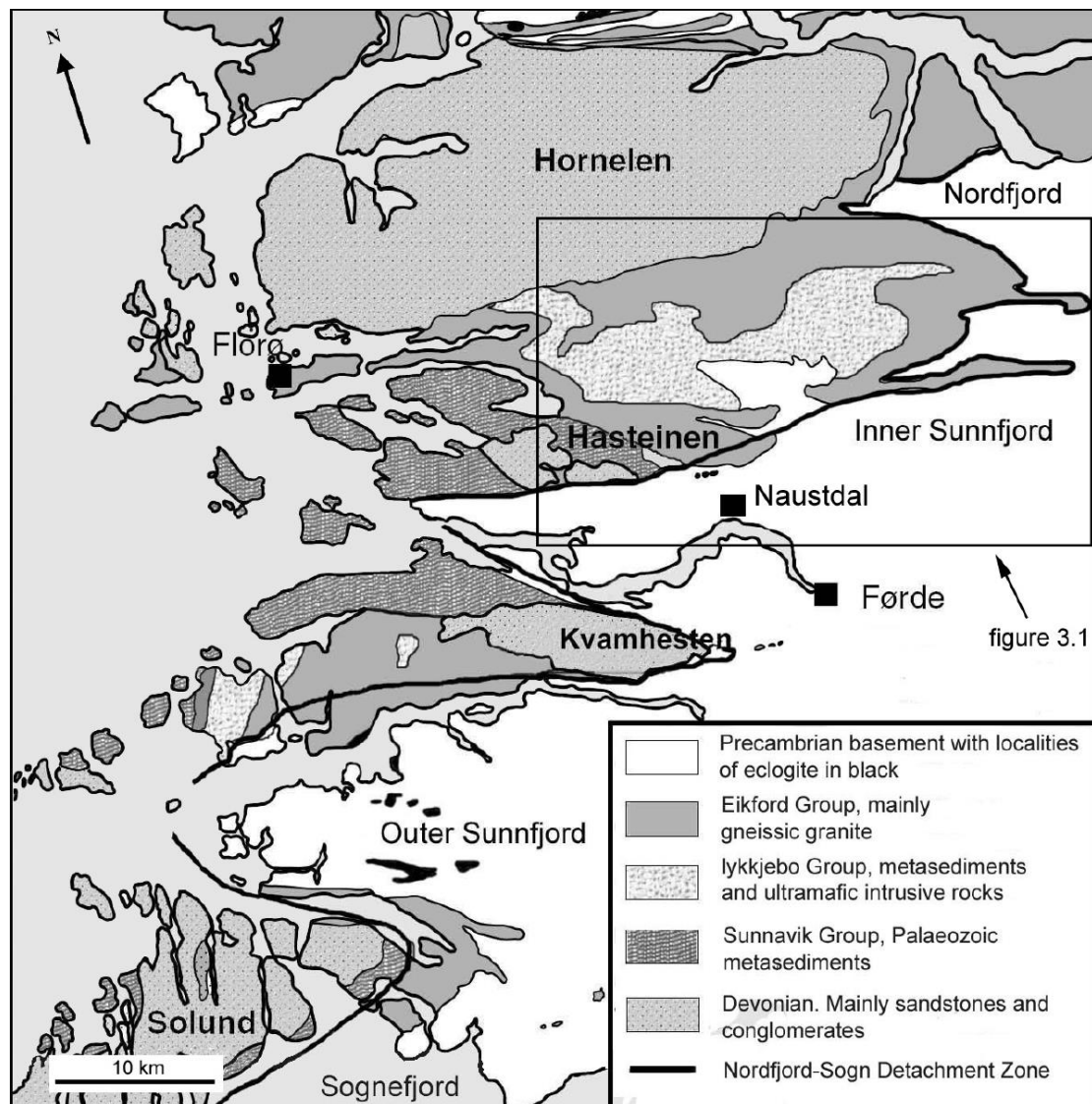


**Figure 2.1:** Schematic geology of part of the Western Gneiss Region altered after geological map/REF (see inset figure 1.2).

The thinned and stretched nappes are situated on top of the (U)HP rocks. The extreme short spatial transition between low grade rocks and the exhumed UHP rocks is not well understood. In the north of the WGR this transition from basement to nappe

shows no such “metamorphic gap” and not only the nappes but also the basement has undergone recrystallization to a lower metamorphic grade.

### 2.1.1 Autochthon-Parautochthon basement

The Baltic Shield is the continental crust of Fennoscandia. In the south it consists of numerous Proterozoic plutonic rocks, migmatites and gneisses, and locally also Mid-Proterozoic supracrustal rocks (Fossen et al., 1992). The main part of the basement is autochthonous however the western part of the Baltic Shield, the Western Gneiss Region (WGR), is internally affected by Paleozoic deformation and metamorphism. It shows an overall increase in intensity of metamorphic grade towards the northwest (Bryhni & Sturt, 1985; Griffin et al., 1985).

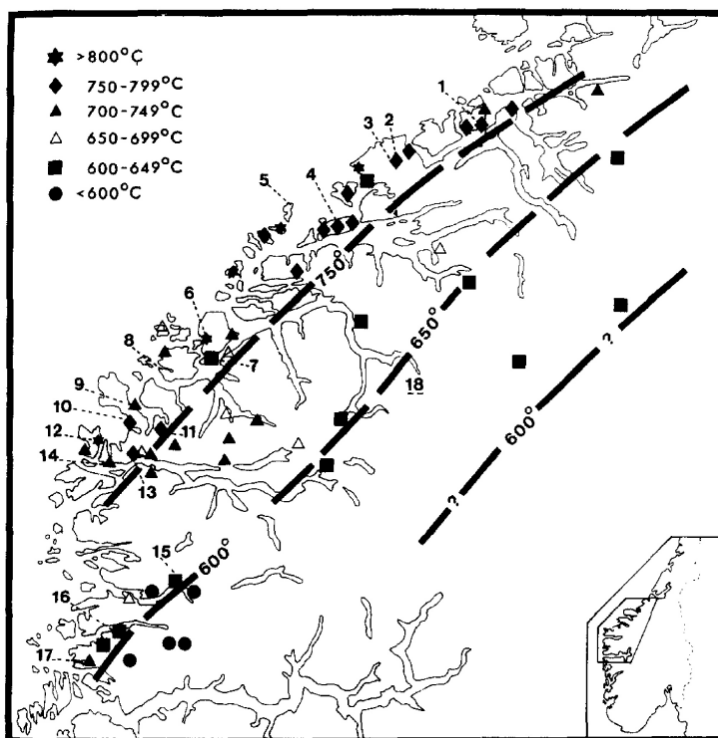


**Figure 2.2:** Map of WGR with eclogite sample localities (Griffin et al., 1985). Eclogite isotherms are calculated from  $K_D = \left[ \frac{(Fe/Mg)_{gnt}}{(Fe/Mg)_{cpx}} \right]$  by method Ellis and Green 1979 at 15 Kbar. After Griffin and Brueckner (1985).

Similarly to the basement of the WGR, the metamorphic grade of cover of the autochthonous basement increases from the foreland region towards the coastal areas in the west. This indicates an originally ESE-characterized wedge-shaped geometry of the Caledonian nappe pile. The eclogites found in the westernmost part of the WGR, fit perfectly in the picture of increasing metamorphic grade from the foreland of the Caledonides towards the coastal area of Norway (figure 2.2).

This increase of metamorphic grade in the WGR towards the west is interpreted as a reflection of the western margin of Baltica subducting below Laurentia to depths of 60- 70 km or more during the Silurian continent-continent collision (Griffin et al., 1985; Hacker et al., 2003), diamonds indicate depths of more than 130 km and with

ultra-high garnet peridotite indicating depths of >185km (Van Roermund & Drury, 1998; Van Roermund et al., 2002).

To the west of the WGR, the basement is part of the passive margin of Baltica and consists of Proterozoic crystalline rocks overlain by Upper Proterozoic rift sediments, Cambrian to Wenlockian shelf sediments, and Upper Silurian molasses (Bockelie & Nystuen, 1985; Hacker et al., 2003).

### **2.1.2 Allochthonous nappes**

These nappes have mostly a Vendian to Ordovician age and have been thrust together with basement, on top of the basement prior to and locally also during the formation of the Scandian orogeny (Fossen & Dunlap, 1998). The nappes are categorized into structurally distinct entities; Lower, Middle, Upper and Uppermost allochthons, which are separated from each other by regionally extensive faults (figure 1.2). The nappes have varying metamorphic grades and show different complex internal deformations and structures (Dallmeyer and Stephens, 1991). The nappes in southern Norway, which are part of the Scandinavian Caledonides, are thin (10 km) but very extensive (50 000 km<sup>2</sup>). They have been emplaced on top of the Precambrian basement and cover in a Southeast-direction over a distance of up to 300 km (Andersen et al., 1998; Fossen & Dunlap, 1998). This displacement is believed to be largely accommodated by the extensive detachment zones that run along the coast of western Norway together with normal faults. These detachments are generally characterized by non-coaxial deformation and mylonite zones and according to Andersen et al. (1994) can be up to several km thick in the Western Gneiss Complex.

The Jotun Nappe is one of the largest thrust sheets on the Baltic Shield. It is a pre-collisional remnant of the continental margin of Baltica that has been displaced on the detachment zone (Fossen & Dunlap, 1998).

#### The Lower Allochthon

The Lower Allochthon consists of low grade sediments of Neoproterozoic to early Palaeozoic age with several nappes being imbricated by basement thrust sheets. An increasing metamorphic gradient is apparent in the sediments from low/medium greenschist-facies in the East of the nappe to amphibolite facies in the most westerly part of the nappe (Roberts & Gee, 1985)

#### The Middle Allochthon

The Middle Allochthon in the Caledonian orogeny mainly consists of deformed plutonic basement complexes including units like the Jotun Nappe Complex, the Lindås nappe, and the Høyvick and Herland groups (Corfu & Andersen, 2002). The Precambrian Jotun and Lindås nappes were formed by several magmatic events between 1700 and 1250 Ma and between 950-900 Ma by a complex Svecnorwegian magmatic evolution (Corfu & Andersen, 2002). Other constituents of the Middle

Allochthon are thick sequences of psammites and Vendian to lower Palaeozoic meta-sediments.

### The Upper Allochthon

This Allochthon consists mainly of ophiolites and island-arc sequences and is an extremely heterogeneous, internally structurally imbricated complex. The lower part, also known as the Seve Nappe complex, is thought to contain fragments of basement and transitional continental-oceanic crust of the rifted margin of Baltica (Roberts and Gee, 1985; Dallmeyer and Stephens, 1991; Brueckner and Van Roermund, 2004).

### The Uppermost Allochthon

The Uppermost Allochthon can only be found in the northern part of Norway and does not border the WGR like the Lower, Middle and Upper Allochthon. It consists mainly of high-grade metamorphic sediments, migmatitic paragneiss, marble and ophiolite of early Palaeozoic ages.

### **2.1.3 Shear zones**

Large scale to northwest and west dipping shear zones rooted in the ductile lower crust run along the coastal range of Norway (Dewey et al., 1993; Braathen, 1999; Andersen et al., 1994; Carswell et al., 2003; Brueckner and Roermund, 2004; Johnston et al., 2007). These extensive shear zones include the Nordfjord-Sogn detachment zone (NSDZ) (figure 2.1) and the Hardangerfjord (HSZ) and are several kilometres in thickness (Andersen et al., 1994; Fossen and Dunlap, 1998).

The NSDZ contains many clear kinematic indicators that show top to the west movement (Fossen and Dunlap, 1998). The expected kinematic indicators for an orogeny that formed during collision between continental plates would be contractional. In the case of the Scandinavian Caledonides, the contractional indicators are overprinted by kinematic fabrics formed during the syn- or post orogenic extension indicating that extension and not convergence was the final tectonic movement in the formation process of the Scandinavian Caledonides.

### **2.1.4 Devonian sedimentary basins**

The Devonian sedimentary basins, also called Old Red Sandstone basins, were formed during extensional detachment faulting accommodating a number of low-grade metasediments like conglomerate, sandstone, shale and limestone (Andersen and Jamtveit, 1990) (figure 2.1).

## **2.2 Western Gneiss Region**

Several Gneiss Complexes are present in the Caledonides of Norway one of which is in the Western Gneiss Region (figure 1.2). Labrousse et al. (2004) found that during the Scandian regional E-W stretching resulted in the formation of a core complex with an extent of 35 000 km<sup>2</sup> in the WGR. This Western Gneiss Complex (WGC) is at present structurally the deepest exposed unit of the Scandinavian Caledonides (Labrousse et al., 2004; Andersen & Austrheim, 2003).

The protoliths of the WGC are dominated by Middle Proterozoic (950 –1800 Ma) orthogneisses (Corfu and Andersen, 2002). These rocks experienced high to ultra-high pressure metamorphic conditions during the Scandian continental collision between Baltica and Laurentia. At an increasing number of localities the high pressure mineral coesite or remnants of coesite have been found (Smith, 1984). Also diamond, indicating depths between 120-130km (temperatures between 700-800 °C), has been found by Dobrizhinetskaya (1995) and Van Roermund et al., 2002.

### **2.2.1 The Nordfjord-Sogn Detachment zone**

The Nordfjord-Sogn Detachment zone (NSDZ) is a detachment zone that runs through the WGC and accommodated the displacement of the allochthonous units now found on top of the WGC (Krabbendam & Dewey, 1998; Corfu & Andersen, 2002; Johnston et al., 2007). Not all of the NSDZ is exposed and so far the zone stretches from the Solund area in the south to the Nordfjord areas north of the Hornelen basin (figure 2.1).

The NSDZ divides the overlying allochthons from the WGC basement and accommodates a large pressure gap between these two units. Rock units that have experienced pressures of c. 20 Kbar are in contact with units which only experienced pressures of 10 Kbar or less (Johnston et al., 2007). In the Kvamhesten basin,  $\geq$  16kbar eclogites occur within 3 km from the Devonian rocks. This metamorphic gap equates to 45-50km of crust. North of the Hornelen basin this gap is even bigger with  $\geq$  20 km eclogite situated within 3 km distance of the Devonian sediments (Osmundsen & Andersen, 2001). Estimates of 50-110 km of displacement along the NSDZ have been made with help of shear-strain calculations and contrasts in metamorphic grade across the detachment (Marques et al., 2007).

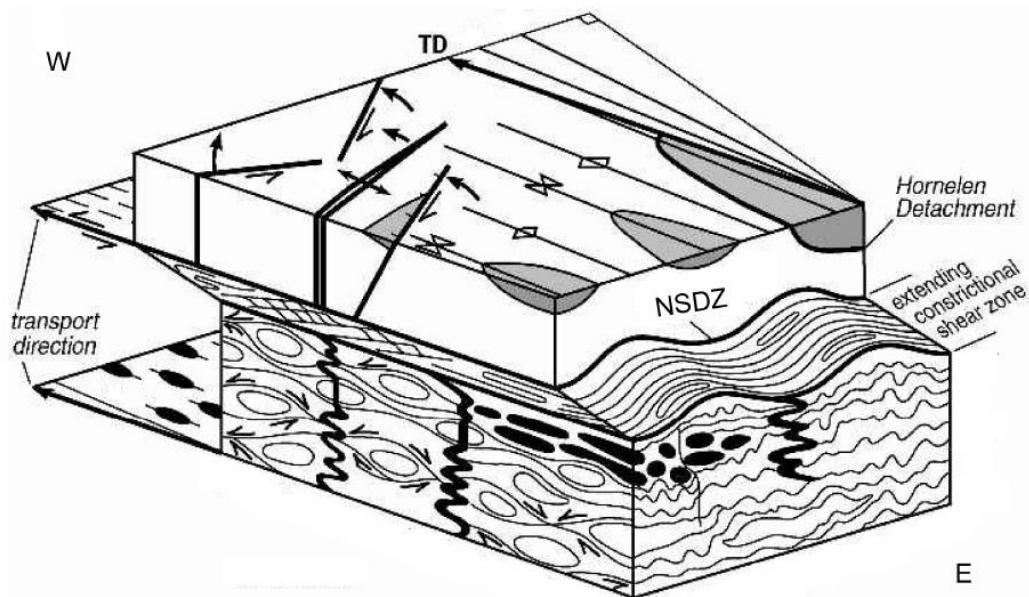


**Figure 2.3:** A Schematic representation of the geometry of structures in the Western Gneiss Region of south-western Norway. TD = detachment slip direction (Dewey, 1993)

In some areas this major jump in metamorphic grade has not been well defined and the relationship between the units becomes less clear. An example of this can be found east of the Hornelen Basin (figure 2.1). Here the NSDZ (possibly) roots in the lower crustal rocks and has not accommodate as much displacement of the nappes as at other parts of the NSDZ. Here, detachments situated at higher structural levels, like the Hornelen detachment, are more likely to have accommodated most of the displacement.

In figure 2.3, illustrates the different shear zones at different structural levels in the WGR. The detachment slip direction is towards the west. The entire crustal section has been folded in a set of NW- and WSW trending folds with amplitudes and wavelengths of several kilometres. The Hornelen basin can be viewed as a west plunging syncline filling progressively eastward as the detachment slipped westward (Dewey, 1993).

The NSDZ is thought to have formed during the Scandian subduction process as a thrust zone. Once convergence between Baltica and Laurentia came to a halt and extension tectonics started, this thrust zone was reactivated as a low-angle detachment zone and subsequently became transected by steeper angled shear zones (Fossen & Dunlap, 1998). A number of these low angle ductile extensional shear zones can be found in the hanging wall of the NSDZ, for example in Sunnfjord and Nordfjord (figure 2.1). It is also found that some shear zones truncate brittle normal faults in the hanging wall of the NSDZ. A good example of this can be found in the Kvamshesten Basin and indicates that the ductile shear zones became active/were still active or were reactivated after brittle deformation of the hanging wall.

Large scale, northwest to west shallow dipping shear zones rooted in the ductile lower crust, accommodated the movement during post Scandian extension. In the brittle

stage of the WGC, normal faults which rooted in the NSDZ, controlled the surface of the crust and the formation of basins. The Hornelen and Kvamhesten Basin formed as a result of these large detachment shear zones (Andersen & Austrheim, 2003).

Ductile deformation is believed to have affected a ca. 2 km thick zone along the NSDZ. Rolled feldspars, shear bands and drag-folds indicate a top to the west extensional movement. Domains outside this shear zone are not affected by this deformation and still contain fabrics related to Precambrian and/or Caledonian events. A second stage of brittle deformation postdates ductile deformation introducing brittle features to the rock. Large brittle extensional faults can be found in and in close proximity of the ductile shear zone which also have a west-vergent signature. Both the ductile and brittle extensional movement are believed to have occurred within one single event and with continuous extension during uplift (Chauvet & Dallmeyer, 1992)

### **2.2.2 Sunnfjord area**

The Sunnfjord area is situated between the Sognefjorden and the Nordfjord in the WGR (figure 2.1). In this area, 4 main tectonic complexes can be distinguished: 1) the Precambrian basement, 2) nappes with Late Proterozoic to Silurian cover, 3) Caledonian ophiolite/ island arc rocks and 4) Devonian sediments. The nappes, ophiolites and Devonian sediments can be found in four different basins which are separated from the basement by the NSDZ. The basins are from north to south; Hornelen Basin, the Håsteinen Basin, the Kvamshesten Basin and the Solund Basin (Hossak, 1984).

This study concentrates on the area north of Naustal, which is a small village south of the Hornelen Basin and to the east of the Håsteinen Basin (figure 2.1). The lowest structural unit in this area is the basement, consisting of gneisses of granitic to grandioritic composition (figure 2.4). Here the basement is covered by several para-autochthonous units which can be subdivided into:

(1) Eikfjord group or Dalsfjord suite is metamorphosed Precambrian intrusive rock consisting of gneissic granite, gneiss emplaced with meta-anorthosite, amphibolite, granulite and augengneiss,

(2) Lykkjebø group or Høyvik group consisting of sedimentary and intrusive rocks of probably late Proterozoic age with mainly metasediments like quartzite, phyllitic schists and mica schists, and ultramafic rocks,

Eclogite lenses can be found within the gneissic basement and the Eikfjord group. The magmatic Eikfjord/Dalsfjord group is unconformably overlain by metasediments of the Lykkjebø/Høyvik group (Andersen et al., 1994).

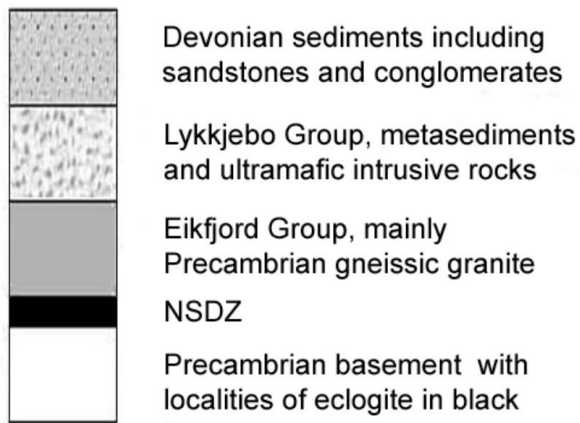


**Figure 2.4:** Tectonostratigraphic section of the Naustdal region. Unit thickness not to scale.

### 3. The basement–nappe contact in the Naustdal region

Four cross sections, representing the contact between the basement and overlying nappe units in the Naustdal region, were studied (fig. 3.1). The cross sections run perpendicular to and through the basement unit, detachment zone and the overlying nappe. Along these cross sections samples were taken and outcrops were described in detail. The samples were used for reference and also made into standard 0.3 mm thick thin sections for analysis.

#### 3.1 Field method

The cross-sections, along which the field observations were made, run from southeast to northwest at a more or less perpendicular orientation to the tectonic stratigraphy and the basement-nappe contact. The location of the cross-sections is based on the geological map (Bryhni and Lutro, 2000). To assess any increase or decrease in structural or metamorphic grade of deformation a significant part of the cross-sections is situated in the basement.

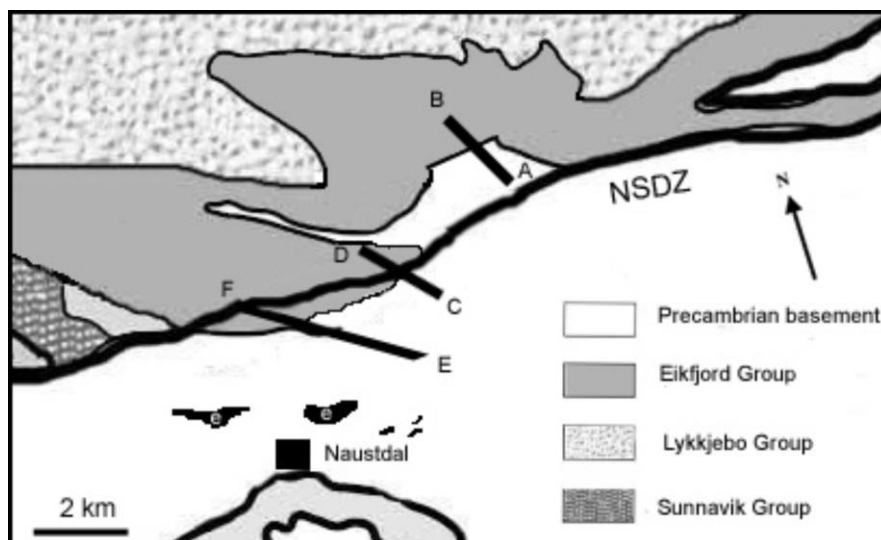


**Figure 3.1:** Schematic geological map of a part of the Sunnfjord area with the three sampling cross-sections marked with a black line: AB) first cross-section including samples ...; CD) second cross-section including samples ...; EF) third cross-section including samples (altered after Bryhni and Lutro, 2000). Samples descriptions can be found in Appendix II

Along the cross-sections, the mineral contents and the rock textures within the basement, detachment zone and overlying nappes, were determined. To determine the shear sense in the basement, detachment zone and overlying nappe, kinematic indicators like rolled feldspars, shearbands and drag folds were used.

#### 3.2 Field observations

In the following section every cross section is discussed separately. A detailed description of every sample-point in cross-sections can be found in the appendix II.

### Cross-section AB:

At this cross section the detachment does not run on the basement nappe contact and is situated to the south of this contact. The cross section starts north of the detachment and crosses the contact between the basement and the nappe. The basement rock closest to the detachment (at point A of the cross-section, figure 3.1) is a granitic compositionally layered gneiss. The layers have either a relative increased mica or feldspar/quartz content.

The layers in the granitic gneiss are folded into 0,1 to 3 meter long recumbent isoclinal folds. These tend to be present in most parts of the basement where it consists of granitic gneiss. Close to the shear zone, the recumbent fold hinges have an EW orientation with little or no dip. The orientation of folds changes to NE/SW towards the end of the cross section (B).

Along the cross-section, the mica contents in the basement rocks vary. At parts of the cross-section, the basement consists of felspathic schist with k-feldspar augen. In these more mica rich parts, layers show little or no folding. The k-feldspar augen however are heavily flattened, stretched and often also rotated indicating top to the west shear movement. Midway through the cross section the rock type changes abruptly from gneiss with varying mica contents to a quartzofeldspatic gneiss with little mica. These rocks have a more fine grained texture.

At the southeast part of the cross section (point A; basement) the foliation is NW- SE and dipping to N/NE (figure 3.2). The samples closer to B show a NE – SW foliation, dipping to N/NW. The orientation of the foliation changes with about 18-30 degrees from A to B. In a similar fashion the foliation lineation also changes from a W/NW direction to W/SW from A to B, becoming less aligned with the shear zone. These orientation changes in foliation and lineation are, similar to the change in rock type, very abrupt and indicate the change from basement to nappe (figure 3.2).

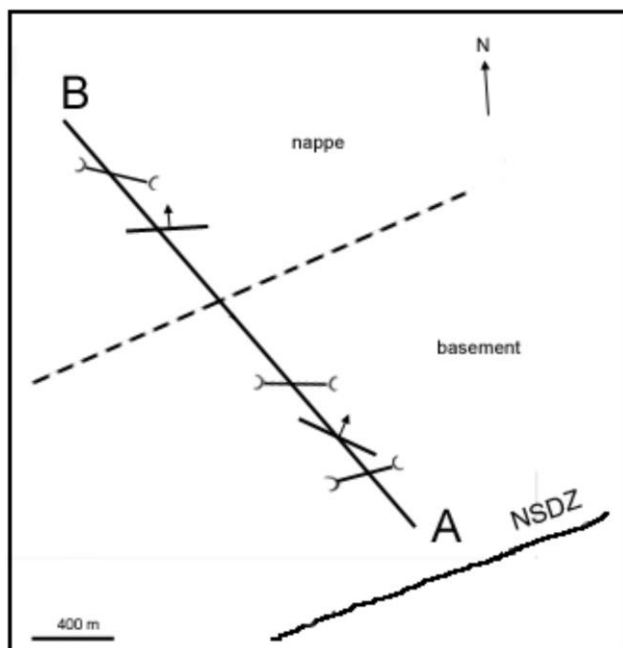


**Figure 3.2:** Schematic drawing of cross-section AB with orientation of foliation with dip-direction and orientation of lineation.

### Cross-section CD:

This cross section starts in the basement (C; figure 3.1). At this point the basement is a granitic gneiss with compositional layering which is folded (figure 3.3). The asymmetric folds are 5 – 30 cm long. Along the cross section the basement varies from augen gneiss to mica gneiss. Feldspar augen throughout the cross section indicate top to the west shear movement (figure 3.4, 3.5).



**Figure 3.3:** [22.9] Basement; granitic to granodioritic gneiss with symmetric folds.



**Figure 3.4:** [17.2] Basement; augengneiss with augen indicating top to the west shear movement.

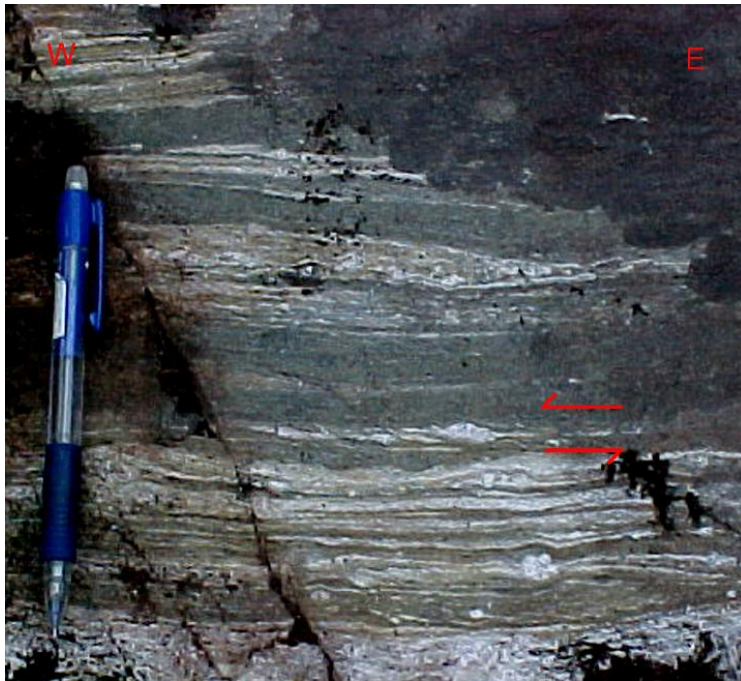


**Figure 3.5:** [22.9] basement; small scale layering and boudinage in granitic gneiss.

A clear change in rock type is apparent midway the cross section. The rock type from there on is a mica schist with locally garnets and feldspar augen and towards the end of the cross section (B) becomes a quarzofeldspatic gneiss. The compositional layering in this quarzofeldspatic gneiss is non-isoclinal (figure 3.6), indicating the transition from basement to nappe.

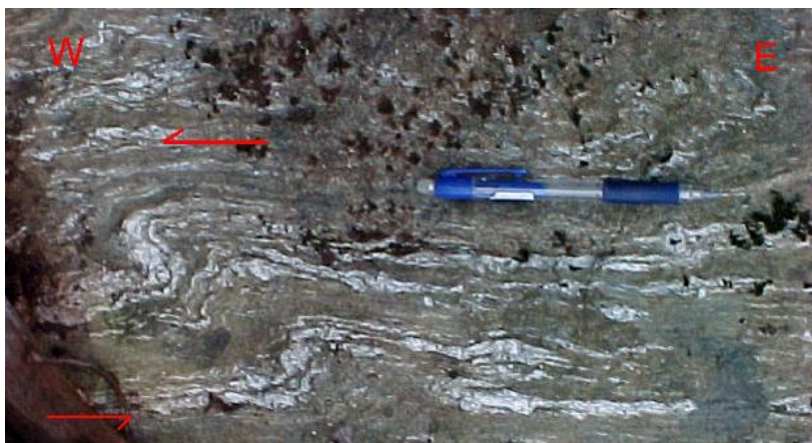


**Figure 3.6:** [22.4] lykkjebo group; quarzofeldspatic gneiss with asymmetric non-isoclinal folds.

The shear zone, separating the basement from the nappe was located using orientations of foliations and lineations (figure 3.7). The foliation furthest away from the NSDZ has a NE/SW orientation which changes to E/W near the shear zone. Towards the shear zone, lineations rotate from an E/W or NW/SE orientation to NE/SW orientation becoming again more parallel to the shear zone.

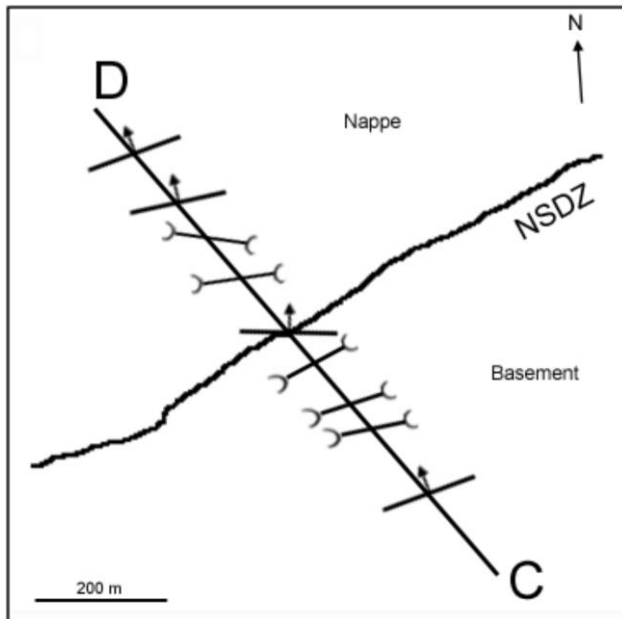


**Figure 3.7:** Schematic drawing of cross-section CD with orientation of foliation with dip-direction and orientation of lineation.

#### **Cross-section EF:**

This cross section does not cross the NSDZ but crosses the nappe-basement contact which is marked by a separate shear zone. The basement in this cross section is similar to that in the other cross sections consisting mainly of augen gneiss. Midway through the cross section the basement is heavily affected by a shear zone separating the basement and the nappe. The basement rocks in the shear zone have a mylonitic texture. The west side of the shear zone is formed of nappe rock consisting of mica schist. This schist is strongly crenulated and consists mainly of chlorite and biotite. Further away from this shear zone and closer to the NSDZ (towards F) this mica schist becomes less crenulated, more muscovite and biotite rich and occasionally contains small garnets.

The foliation and lineation (figure 3.8) also indicate the presence of a shear zone in the middle of the cross section. In the shear zone, the foliation is at a more east west orientation than anywhere else in the nappe and basement. The lineation becomes parallel to the orientation of the shear zone whereas in the rest of the cross section the lineation has an E/W orientation. Closer to the NSDZ the lineation becomes parallel to the orientation of the NSDZ.

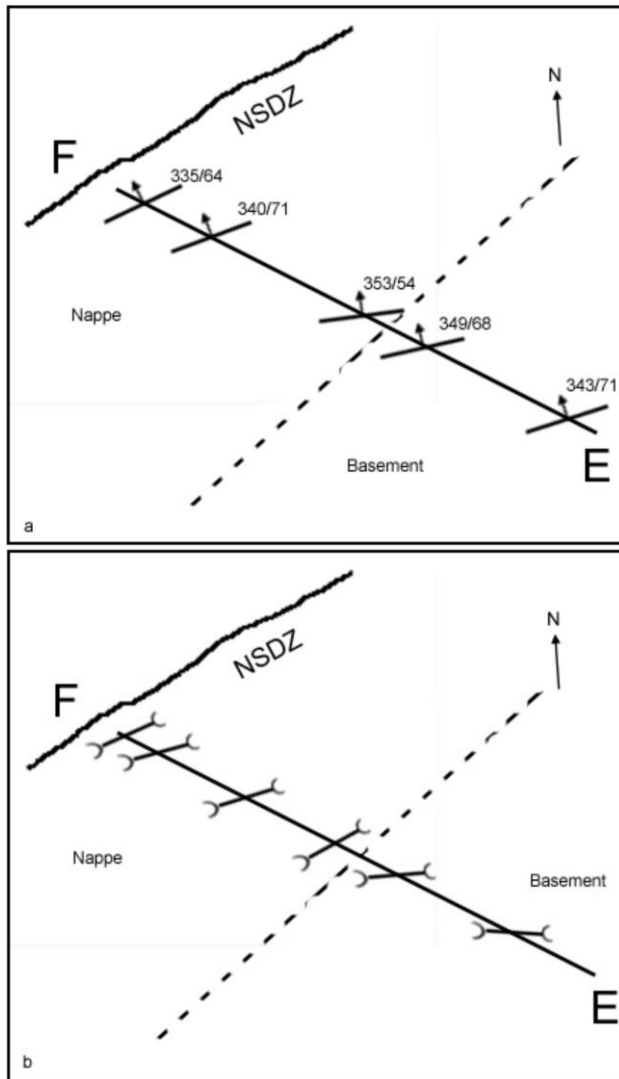


**Figure 3.8:** Schematic drawing of cross-section CD with a) orientation of foliation with dip-direction and b) orientation of lineation

### 3.3 Petrographic analysis

Petrographic micro-structures and mineralogy of all samples from the three cross-sections were analysed using optical microscope. Sampling started at the base of the tectonic stratigraphy and continued into the lower nappe units. In the following, a general description is given of samples from every individual cross-section. Photo's of the thinsections are filled in Appendix III.

#### **Cross-section AB:**

The average grainsize of rock samples decreases and becomes more homogeneous towards the end of the section (B, figure 4.2) in the north. All samples have undergone feldspar recrystallization but the average grainsize highly depends on the extent to which feldspar crystals have been broken down. The texture of the matrix becomes more symmetric towards the nappes with the two samples collected from the nappes having only symmetric micro-structures. In the basement mica's become increasingly asymmetric. Feldspars in samples 18.7 and 18.8 (close to A) also are

more asymmetric with the latter having even increased asymmetry. The sample at A is also characterized by increase in fractured feldspars crystals which in some cases have undergone “bookshelf” rotation. This latter sample furthermore contains feldspars showing asymmetric tension gashes.

Every rock sample from this section, with the exception of sample 3.1 and 3.3, contains amphibole and chlorite. However, a decrease in amphibole volume % from sample 18.8 to 18.6 is apparent which is further away from the NSDZ. The amphibole is assumed to have formed under amphibole facies conditions where recrystallization took place. As such the volume % of amphibole present in the basement rock is an indicator of the amount of recrystallization which took place under amphibolite facies conditions. Most amphibole crystals show signs of brittle deformation indicating that deformation continued at lower pressure and temperature. Continued deformation provided conditions where chlorite was able to form in the cracks after or during brittle deformation.

### **Cross-section CD:**

Rocks from the basement, south of the main detachment (NSDZ), have asymmetric micro-structures. Sample 22.7 is a pseudotacholite which is believed to represent the detachment between the basement and the nappes. Nappe samples from north of the detachment indicate little retrograde metamorphism in chlorite facies. Micro-structures of these samples also lack the asymmetry found in the rock samples from the basement. Even though there is a difference between the matrix of rock samples from the nappe and basement, all samples contain porphyroblasts which indicate top to west kinematics (figure 3.9).



**Figure 3.9:** Thinsection of sample .. from cross-section CD with porphyroblasts indicating top to the west kinematics.

### **Cross-section EF:**

In cross section EF, the sample at E is the only basement sample and is an augen-gneiss with no amphibole but small garnets and small amounts of mica's. The matrix shows hardly any asymmetric shear sense indicators. The sample from the detachment is almost mylonitic with large amounts of chlorite and quartz evident of

recrystallization in chlorite facies and deformation by shearing. A nappe sample at only a small distance from the shear zone (200 meters) has undergone less recrystallization in the chlorite facies and contains more minerals like biotite, epidote and feldspar. Closer to the shear zone, samples from the nappe show increasingly asymmetry in the micro-structure of the matrix. Towards the end of the cross-section and close to the NSDZ (in the nappe, F) the rocks show less signs of recrystallization in chlorite facies and subsequently the metamorphic grade increases to amphibolite facies.

### 3.4 Summary of observations at the basement- nappe contacts in the Naustdal region

Most rocks along the cross sections show compositional layering most of which is intensely folded associated with deformation. In the basement, folds are isoclinal in gneisses with low mica content indicating extensive deformation. The k-feldspar augen which often can be found in gneisses are used as shear-direction indicators and in every cross section indicate a top to the west shear movement in the basement. Not only basement close to the detachment is affected by this shear movement but also at larger distances (> 2 km). However, significant change in the orientation of foliation and lineation can only be noticed within 1 km of the detachment.

In the AB cross section, shear movement concentrated in the NSDZ which affected the basement in close proximity to this detachment. The nappe is in this area not affected by the movement along the shear zone and no shearing occurred on the basement – nappe contact itself.

In the CD cross section most of the extensional shear movement along the NSDZ is concentrated in the basement and only to a lesser extend in the nappe. Firstly this follows from the lineation orientation in the basement which is more parallel to the NSDZ whereas the lineation in the nappe has retained a NW/SE orientation. Secondly, the micro-structures in the rock indicate that the basement rocks have undergone top to the west shearing whereas microstructures or nappe rocks show no asymmetric kinematics.

In cross section EF the shear displacement did not focus only in the NSDZ but occurred also along a second shear zone on the border of the basement and nappe. The mineral alterations suggest that this shear zone was active at greenschist facies during which biotite was altered to chlorite.

## 4. Monazite geochronology

### 4.1 Introduction

Monazite is a lanthanum-cerium light rare earth element (LREE) phosphate with the general formula of (LREE)(PO<sub>4</sub>) (Nriagu and Moore, 1984).

It occurs as an accessory phase in felsic magmatic rocks, moderate to high-grade metamorphic rocks (450-600°C) and as a detrital mineral in sedimentary rocks (Foster, 2000; Foster et al., 2002; Giles and Nutman, 2002). Good examples are pelitic schists or felsic rocks metamorphosed to amphibolite or even granulite facies. This rock type is likely to prevent any growth of amphiboles and garnets, which are both known to take up significant quantities of REE preventing monazite growth (Wing et al., 2003).

The monazite mineral consists of a group of endmembers defined by the dominant LREE present in the monazite. These including (Ce)-monazite, (La)-monazite, (Nd)-monazite and (Sm)-monazite. The most common endmembers, (Ce)-monazite and (La)-monazite, are known for their relative high thorium and uranium content (Foster et al., 2002). Because the non-radiogenic lead (Pb<sup>204</sup>) incorporated in the mineral during its growth is negligible, all measured lead (Pb<sup>207,208</sup>) in monazites must be correlated to the decay of uranium and thorium.

However, at conditions with temperature of >750-800°C, uranium, thorium and lead undergo volume diffusion in monazite (Cherniak et al., 2004; Gibson et al., 2004). Of these two elements, Pb has the lowest closure temperature and therefore is the constraining factor in the U-Th-Pb system. Under dry crustal conditions, for example, Pb is predicted to be immobile and volume diffusion of Pb in monazites is largely irrelevant in the U-Th-Pb system (Cherniak et al., 2004).

The closure temperature is defined by Dodson (1973) as “the temperature of a system at the time of its apparent age”. In other words it is the temperature below which the isotopic clock is switched on and there is no diffusion out of the system. The closure temperature is given by:

$$T_c = R / \left[ E \ln \left( A \tau D_0 / a^2 \right) \right]$$

In which R is the gas constant, E the activation energy,  $\tau$  the time constant with which the diffusion coefficient D diminishes, a is a characteristic diffusion size, and A a numerical constant. The time constant  $\tau$  is related to cooling rate by:

$$\tau = -RT^2 / (EdT / dt)$$

The closure temperatures for monazite, where volume diffusion of Pb becomes negligible, are found to be between 750-800 C (Bingen & Breemen, 1998).

At temperatures above the closure temperature, monazite is no longer a closed system and the U-Th-Pb system can be reset because Th, U, Pb can diffuse out of the system. In the case where the metamorphic temperature exceeded the closure temperature diffusion of lead is possible and it may be assumed that all lead will leave the system. At the point where the rock cools down to closure temperature the diffusion of lead in

monazite will be blocked and the monazite crystal becomes a closed system. However, it has to be noted that other process like fluid movement in the rock are also capable of resetting the system. Under dry conditions volume diffusion of Pb is the main mechanism by which the system is reset of Pb. However, under wet conditions grain boundary is a very efficient and the predominant mechanism of Pb diffusion in monazites. Under these conditions, the amount of fluids and the chemistry of the fluid involved are likely to be more important controls than temperature (Teufel & Heinrich, 1997).

The closure temperature is likely to depend on a number of factors of which one is the bulk rock chemistry as well as the composition and morphology of individual monazites grains and the duration to which the rock has been exposed to temperatures above the closure temperature hence to what extend the Uranium/Thorium content of monazite could reach equilibrium with the surrounding system.

Because monazite can grow under prograde conditions and because it has a relative high U and Th content (Parrish, 1990), it is an ideal mineral to use for dating rocks, determining metamorphic paths and geochronology using the EMP monazite age dating technique (Wing et al., 2003).

Another advantage of using monazite for this purpose, is that decay radiation does not damage monazite. Phosphate minerals are extremely resistant to the recoil of heavy nucleus following alpha decay (Cherniak et al., 2004)

## 4.2 Sampling strategy

More than 70 samples were collected along three cross- sections across the basement and nappes in the Naustdal area for EMP monazite age dating purposes. The three cross-sections (AB, CD and EF in figure 4.1), with a length of 1-2 km, start in the basement and end in the allochthonous nappes. The mineral content of the rock was used as a guidance for sampling. Moderate to high grade metamorphic felsic rocks were preferred and any felsic rocks containing amphiboles or mafic minerals were avoided. Secondly, high grade metamorphic schists containing garnet were also sampled.

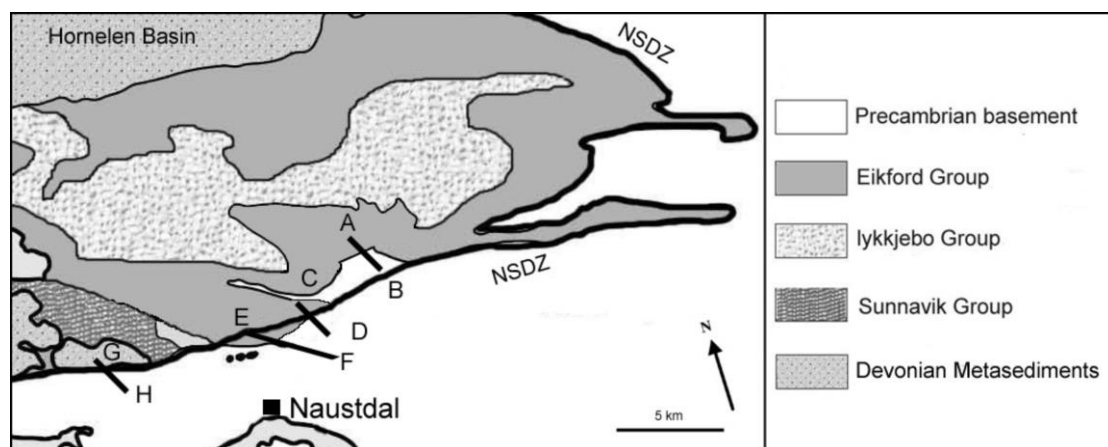


**Figure 4.1:** Schematic geological map of a part of the Sunnfjord area with the three sampling cross-sections marked with a black line: AB) first cross-section including samples ...; CD) second cross-section including samples ...; EF) third cross-section including samples ...

### 4.3 Analytical method

Chemical analysis of the monazite was undertaken with a electron microprobe (EMP), a JEOL JXA-8600.

The monazite grains were located with back-scatter electron microscopy and then qualitatively analysed with energy dispersive spectrometer (EDS) over an elapse time of 20 s to confirm the monazite composition of the grain. Quantitative analysis were then carried out with five wavelength dispersive spectrometers (WDS) with an acceleration voltage of 20 kV, beam current of 50 nA, spot size of 5  $\mu\text{m}$ . Counting times (peak + background) were 240 s for Pb, 200 s for U, and 40 s for all other elements. Overall it took 15 minute for one analysis. The EMP was calibrated with a monazite standard with an age of 175 Ma. The X-ray lines used for an element during a WDS analysis are given in table 3.1. Rough data was then corrected according to conventional ZAF method.

Element	Measurement line
light elements (Ca, P, Si, Al, Mg)	$K_{\alpha}$
most REE, Ba and Sr	$L_{\alpha}$
Pr	$L_{\beta}$
Th and Pb	$M_{\alpha}$
U	$M_{\beta}$

Table 3.1: X-ray lines used during the WDS analysis

Uncertainties (calculated from  $2\sigma$ ) under the chosen analytical conditions were typically  $\pm 1.36$  wt % for Th,  $\pm 3.46$  wt% for U and  $\pm 3.98$  wt % for Pb. Measurements with standard deviation of more than 13 wt% are excluded from the results on the basis that the data from these analysis is not likely to be reproducible.

### 4.4 Age calculation technique

#### 4.4.1 Apparent age (t)

To calculate the apparent age from Th, U and Pb oxide wt % the following equation is used:

$$\frac{PbO}{W_{Pb}} = \frac{ThO_2}{W_{Th}} (\exp(\lambda_{232}t_1) - 1) + \frac{UO_2}{W_U} \left[ \frac{\exp(\lambda_{235}t_2) + 137.88 \exp(\lambda_{238}t_3)}{(137.88 + 1)} - 1 \right]$$

$$W_{pb} = 224$$

$$W_{Th} = 264$$

$$W_U = 270$$

$$\lambda_{232} = 4.9475 * 10^{-11} \text{ y}^{-1} \text{ (Steiger and Jäger, 1977)}$$

$$\lambda_{235} = 9.8485 * 10^{-10} \text{ y}^{-1} \text{ (Steiger and Jäger, 1977)}$$

$$\lambda_{238} = 1.55125 * 10^{-10} \text{ y}^{-1} \text{ (Steiger and Jäger, 1977)}$$

With this equation it is assumed that there is no initial Pb<sup>204</sup> in the monazite grain and the system has been closed since the apparent cooling age “was frozen in” and hence has not been subjected to any volume diffusion of lead, uranium or thorium or any other process that could reset the system. For this reason the data retrieved from the analysis are considered to be concordant.

#### 4.4.2 Isochron age (T / T<sub>0</sub>)

To investigate if any age populations are present in the samples and if so, to calculate accurate population mean ages, the isochron age method is used (Suzuki and Adachi, 1991). In this method the Pb oxide wt% of every individual monazite grain analyzed, is plotted against the amount of apparent Th oxide wt% (ThO<sub>2</sub>\*). The apparent ThO<sub>2</sub>\* value is calculated by converting the UO<sub>2</sub> content into an equivalent amount of ThO<sub>2</sub> produced in the same time (t) period. This recalculated ThO<sub>2</sub> is then added to the measured ThO<sub>2</sub> in the grain to give ThO<sub>2</sub>\*.

The ThO<sub>2</sub>\* value is calculated with the following equation (Suzuki and Adachi, 1991):

$$ThO_2^* = ThO_2 + \frac{264UO_2}{270(\exp(\lambda_{232}t_{app}) - 1)} \left[ \frac{\exp(\lambda_{235}t_{app}) + 137.88 \exp(\lambda_{238}t_{app})}{(137.88 + 1)} - 1 \right]$$

After plotting all analysis, a best-fit regression line is drawn. The isochron age is then calculated from the slope of this regression line with the equation:

$$T_{isochron} = \frac{1}{\lambda_{232}} \ln \left[ \frac{W_{Th} PbO}{W_{Pb} ThO_2^*} + 1 \right]$$

## 4.5 Results

### 4.5.1 Samples with monazites

Only two rock samples from only one cross-section have been found to contain monazite crystals. Two samples, 22.5 and 22.9 contained monazite which are both from cross-section CD (figure 3.1). The rock composition of both samples is very different and will be described here.

Sample N22.5 is a dark grey meta-sedimentary mica schist with a composition of biotite, muscovite, quartz, feldspar. Most of the feldspar occurred as porphyroclasts (~0,5 cm in size). The mica crystals are relative large and exhibit crenulation around the feldspar augen Other porphyroclasts are present in the form of garnet with size ranging from 0,1-0,5 cm). The sample was collected on cross-section 1 (see figure ).

Sample N22.9 is a light grey mica gneiss with 0,2- 4 cm large porphyroclasts of K-feldspar. The rock shows compositional layering of a few mm. This layering is strongly folded at mm scale and incorporating quartz veins that are isoclinal folding.

The monazites in both samples are no larger than the 35  $\mu\text{m}$  in diameter. The more numerous monazites of sample 22.5 are in the range of 10-35  $\mu\text{m}$  in diameter with an average of 21 $\mu\text{m}$ . Sample 22.9 contains not only less monazites but also smaller monazites with a diameter between 10-20  $\mu\text{m}$  and an average of 12  $\mu\text{m}$ . The monazite grains of sample 22.5 are almost twice the size of those in sample 22.9.

Monazites are also often associated with phosphor rich minerals such as apatite. In sample 22.5, monazite can be found in and on the grain boundary of apatite. This type of monazite formed as a thin layer on the apatite grain or as narrow veins running through the apatite grain. These layers or veins are on average only 2-4  $\mu\text{m}$  in thickness.

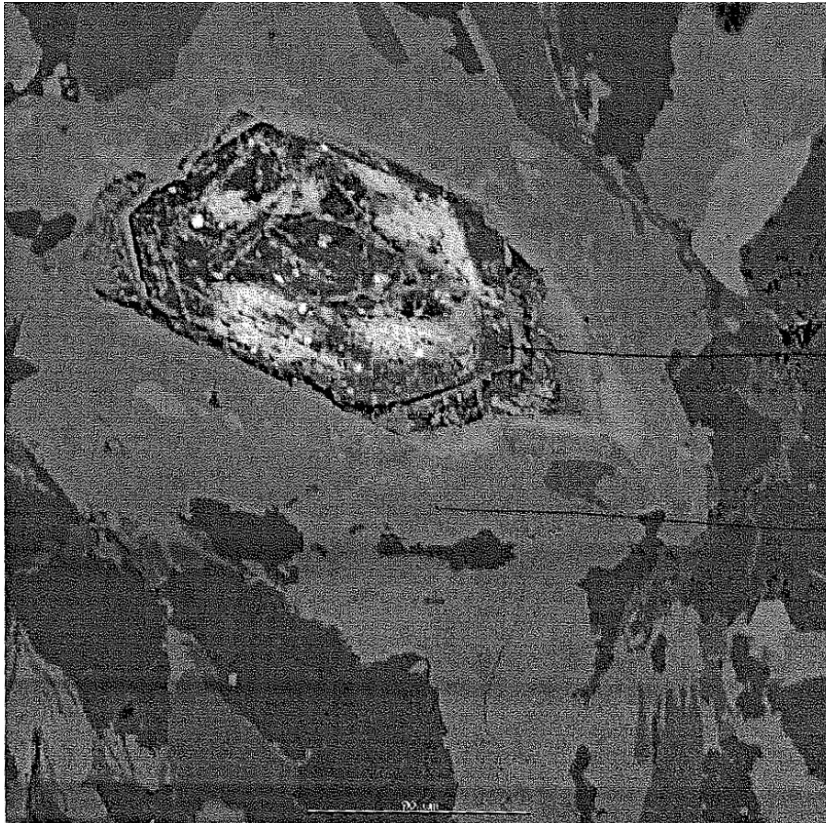


**Figure 4.1:** Microprobe image of a breakdown product of presumably monazite (110  $\mu\text{m}$ ).

Two other samples, 21.6 and 22.1, show presumably breakdown products of monazites (figure 4.1 and 4.2). These remnants have very high phosphor and trace element content and are usually surrounded by grains of apatite.

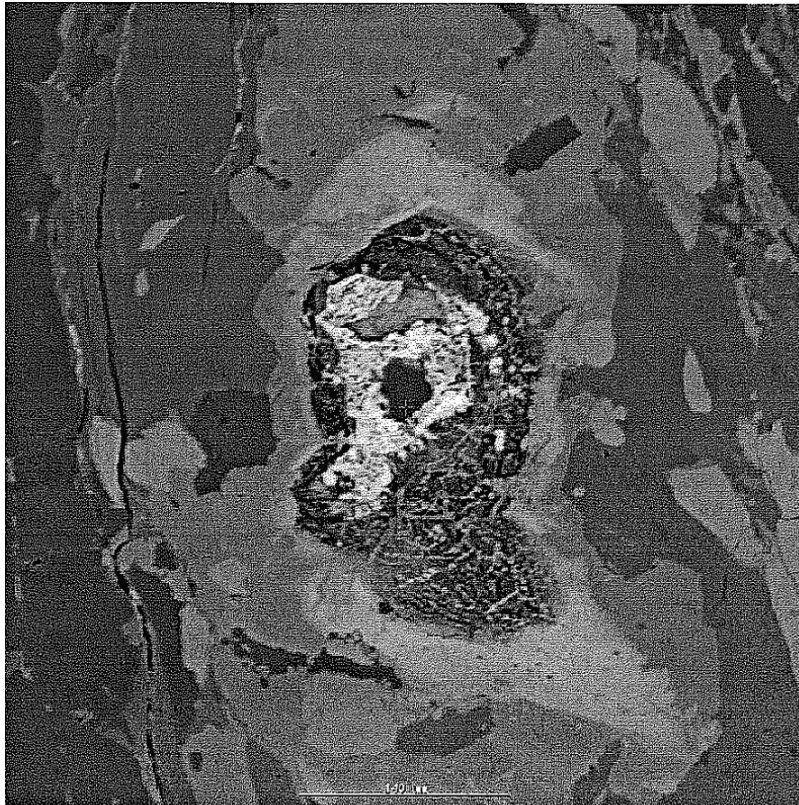


**Figure 4.2:** Microprobe image of a breakdown product of presumably monazite (80  $\mu\text{m}$ ).

#### 4.5.2 WDX analysis of monazites

The chemical composition of monazites from samples 22.5 and 22.9 are given in table 4.1 and 4.2. Sample 22.5 is characterized by monazite-(Ce) which has a relative high Ce content (Appendix IV). In sample 22.9 only the lanthanum end-member of monazite was found with  $\text{La}_2\text{O}_3$  concentrations between 16.98 – 36.14 wt% (Appendix IV). In both samples exists a strong correlation between the measured oxide total and the phosphor concentration where the phosphor concentration in monazites increases with the total oxide weight percentage (figure 4.3).

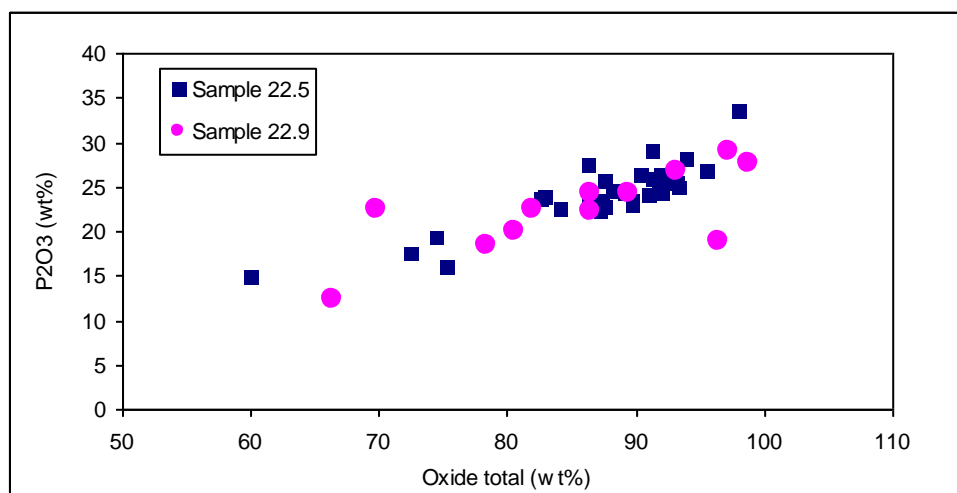


**Figure 4.3:** Total oxide content plotted against the phosphor content in monazites of sample 22.5 and 22.9.

Some monazite measurements have a relative low oxide weight percentage. According to Naggy (2002) only monazites with oxygen totals of 97.5 wt% or more can be assumed to be true monazites. In this study, the sometimes very small grain size of monazites resulted in low oxide weight percentage. Where monazites are smaller than 5  $\mu\text{m}$  in diameter, which is the microprobe spot-size use for the measurements, the measurement incorporates the minerals bordering the analyzed monazite. With a limited number of elements measured by the microprobe during a monazite analyses, element compounds from bordering minerals can account for “the missing” oxygen’s.

In this study, a minimum oxide weight percentage of 95 wt% was used for the calculation of the apparent age to exclude any unsuitable monazite measurements from further age calculations. Due to a lack of good samples with high enough thorium contents ( $>0.1$  wt%) and weight percentage ( $>95$  wt%) for the isochron age calculation a minimum weight percentage of 90 wt% was used.

For the measurements from sample 22.5 with oxide weight percentages of  $>90$  wt% the measured  $\text{ThO}_2$  concentrations range between 0.272- 2.675 wt% which is similar to the  $\text{UO}_2$  contents (0.366 – 2.218 wt%) (table 4.1).

Measurement	PbO	ThO <sub>2</sub>	UO <sub>2</sub>	Total oxide weight percentage
m5N22.5	0.104	1.062	1.316	93.945
m7N22.5	0.189	1.116	1.19	92.19
m2N22.5	0.024	1.733	0.366	98.071
m4N22.5	0.019	0.313	0.55	90.334
m15N22.5	0.127	0.567	1.063	91.775
m16N22.5	0.097	0.586	0.954	92.034
m22bN22.5	0.103	1.378	1.058	95.503
m24aN22.5	0.022	0.272	0.442	91.307
m24bN22.5	0.071	0.929	0.626	93.134
m24b2N22.5	0.066	1.063	0.681	93.352
m24cN22.5	0.059	0.954	0.649	92.977
m26N22.5	0.051	0.356	0.493	91.063

Table 4.1 : Geochemical data of monazites in sample 22.5

In sample 22.9  $\text{ThO}_2$  content of these measurements (oxide weight percentage  $> 90\%$ ) are much lower (0.002- 0.095 wt%). Similarly, the  $\text{UO}_2$  content is also lower with concentration between 0.004 – 0.95 wt% (Table 4 ).

Measurement	PbO	ThO2	UO2	Total oxide weight percentage
m2bN22.9	0.986	0.052	0.191	97.213
m2cN22.9	0.458	0.095	0.004	96.413
m2dN22.9	0.791	0.035	0.16	93.097
m2eN22.9	0.086	0.382	1.063	98.723
m7N22.9	0.737	0	0.615	96.885
m8N22.9	0.826	0	0.449	93.174
m9N22.9	0.671	0	0.219	95.034
m16N22.9	0.513	0	0.18	92.646
m17N22.9	0.548	0	0.148	93.804
m1N22.9a	1.534	0	0.173	95.148
m3N22.9a	1.353	0	0.461	90.701
m4bN22.9a	0.668	0	0.265	90.343

Table 4.2: Geochemical data of monazites in sample 22.9

### 4.5.3 Apparent age

The apparent age, calculated with the method described in the previous chapter, of monazites from samples 22.5 and 22.9 have been plotted in figure 4.4 and 4.5. Only one measurement from sample 22.9 and two measurements from sample 22.5 had a oxide weight percentage of >95 wt% and a thorium content of > 0.1 wt%. The monazite from sample 22.9 gives an apparent age of 519 Ma and the monazites from sample 22.5 give apparent ages of 497 and 195. The latter measurement however has a very low uranium contents (figure 4.5) and will therefore not be considered any further. Furthermore, following the error derivations of Harings (2005) for a Jeol JXA 820 Microprobe at 95% sigma 2 level, errors vary between around 40 to 70 Ma for a single spot analysis.

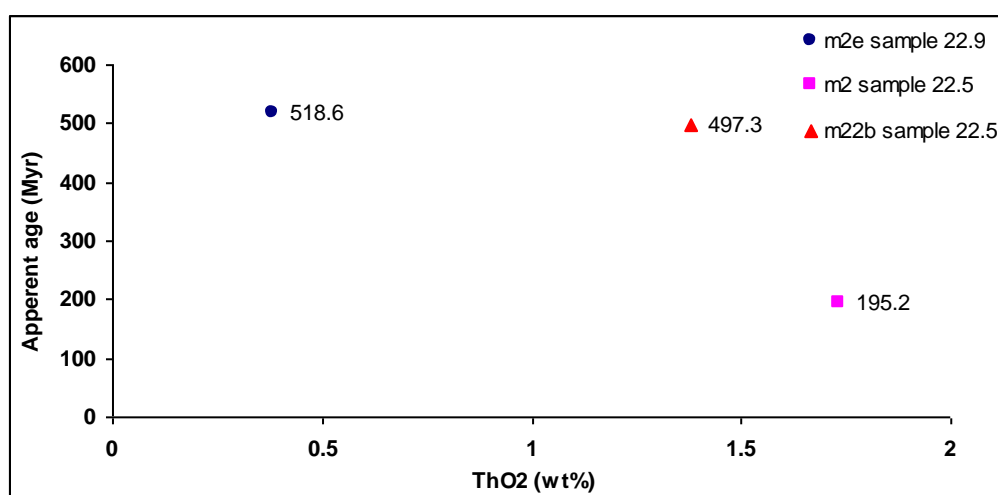
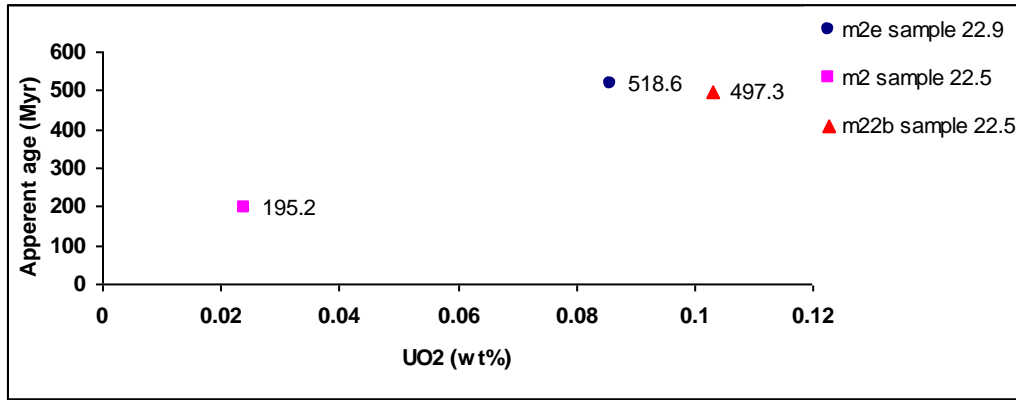


Figure 4.4: Calculated apparent ages plotted against thorium concentration in monazites from samples 22.5 and 22.9.



**Figure 4.5:** Calculated apparent ages plotted against uranium concentration in monazite from samples 22.5 and 22.9.

#### 4.5.4 Isochron ages

The isochron ages represent the apparent age that dominates throughout the monazite population. For determining the isochron ages, a negligible initial lead content is assumed which results in an isochron which intercepts the Y-axis at zero. Due to the lack of good measurements with weight percentages of >95 wt% and ThO<sub>2</sub> contents of > 0.1 wt%, samples with a weight percentage of > 90 wt% have also been included for determining the isochron age. The thorium content in all these samples is > 0.1 wt%. The weight percentage of PbO in monazites is plotted against that of the ThO<sub>2</sub>\* (figure 4.6) between which a linear relationship is assumed. The monazites of samples 22.5 give an isochron age of 557 Ma. The single measurement of sample 22.9 plots also on this linear relationship. This age is slightly higher than the apparent age of sample 22.5.

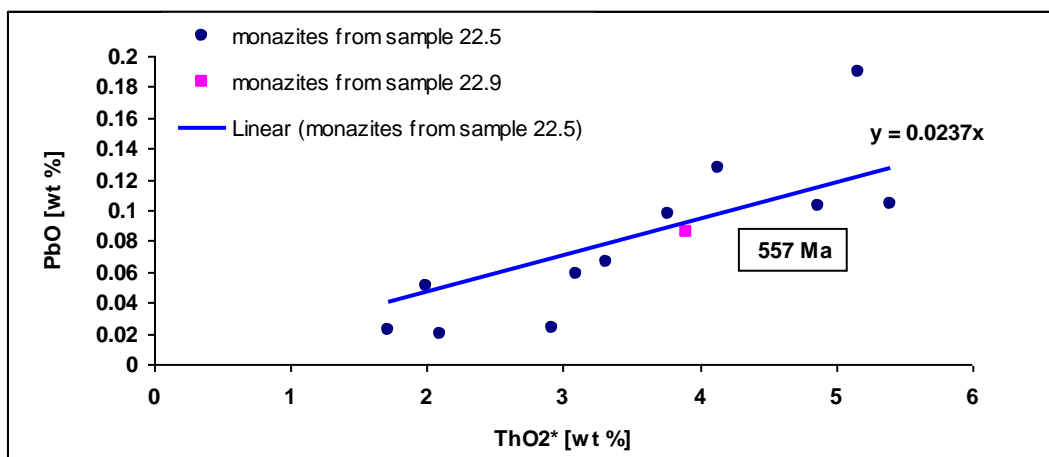


**Figure 4.6:** Isochron ages calculated from PbO and ThO<sub>2</sub>\* weight-percentages in monazite: monazites from sample 22.5 are in blue (circle) giving a isochron age of 557 Ma; monazite from sample 22.9 is in pink (square).

## 5. Discussion

### 5.1 Recap of observations and results

In the Naustdal region the foliation has generally a NE-SW orientation and the lineation has a NW-SE orientation. The field observations showed that along all the three cross sections the orientations of the foliation and lineation change as a result of the detachment. Along the cross section AB, the foliation and lineation are most rotated closest to the NSDZ. Similarly, rocks closest to the NSDZ have asymmetric textures indicating top to the west which gradually change into symmetric textures in rocks further away from the detachment. Feldspar augen close to the detachment are more fractured. The basement rocks furthermore contain amphibole which is not present in the recorded part of the nappe units. The amphibole content decreases with increasing distance from the NSDZ. Most of the amphibole is fractured, especially in rocks closest to the NSDZ.

Rocks from the basement are characterized by up to 3 meter long recumbent isoclinal folds which results from intense shearing. Asymmetric rock textures in the form of asymmetric feldspar augen give top to the west movement and indicate top to the west shearing along the NSDZ under gneiss conditions. During exhumation top to the west displacement continued. Under amphibolite conditions amphibole formed, particularly at shorter distance from the detachment. Continuing movement or reactivation of the detachment at lower PT conditions caused the amphibole to fracture. Bookshelving of amphibole crystals indicates top to the west movement also at lower PT conditions.

The basement-nappe contact in the AB cross-section is not characterized by the detachment. On the contact the foliation and lineation abruptly change by about 20 to 25 degrees which is accompanied by an abrupt change in rock composition. The contact between the basement and nappe is apart from being evident through a compositional change also visible by a fault which runs along the contact. This fault is characterized by brittle fractures filled with chlorite indicating low temperature/pressure activity under chlorite conditions.

In cross section CD, the basement has a gneissic composition whereas the nappe has a schistic to quartzofeldspatic composition. No gradual change in symmetry of the rock texture seems to occur with changing distance from the detachment. Both the basement rocks to the south of the detachment and the nappe rocks to the north of the detachment have asymmetric feldspar augen indicating top to the west shearing. The cross section on either side of the detachment is no longer than one kilometre and therefore it is possible that the cross section is too short to record any transition to symmetric macro-textures. The micro-textures of the basement rocks are all asymmetric whereas the micro-textures of the nappe are symmetric. The rocks on the detachment consist of a pseudotacholite with chlorite filled fractures.

In this cross section, two samples contained monazites. Sample 22.5 from the nappe north of the NSDZ was a mica schist with feldspar augen and small garnets. The second sample, 22.9 from the basement south of the NSDZ is a mica gneiss. Both samples were collected around half a kilometre on either side from the detachment. The sample from the basement gave a monazite apparent age of 519 Ma and the

sample from the nappe gave a monazite apparent age of 497 Ma. The difference between the two ages is 22 Ma. However, there are only a few accurate enough measurements to show a difference in apparent age between the nappe and the basement. Even with multiple spot monazite analysis, monazite ages are rarely identical but tend to spread by as much as 30 Ma (Bingen & van Breemen, 1998). It is argued that components available or involved and recrystallization of metamorphic monazite are the most important processes that control the age variation/spread. As mentioned earlier, in the case of a single spot analysis the error on the apparent age of a monazite at a 95% (sigma 2) level can vary from 40 to 70 Ma. For this reason it is not possible to make a distinction in age between the nappe and the basement.

The isochron for monazites in sample 22.5 (figure 4.3) gave a slightly higher age, 557 Ma, than the apparent age. The monazite analysis of sample 22.9 also plots within the isochron trend of sample 22.5.

At least two episodes of monazite growth have characterized the units in the Naustdal area. The first episode as mentioned earlier is related to the Finmarkian. During the second episode monazite is formed along apatite grains. This secondary monazite, which is present in sample 22.5, could have formed at the lower end range of monazite growth temperatures or under hydrothermal conditions. Apatite is a great source of phosphorus which is the main component in monazite. This might have catalyzed the reaction of monazite. Detachments are often associated with hydrothermal metamorphic reactions and mineral formation. Shearing along the detachment could have created the conditions for the formation of the secondary monazite. This, along with the field observations, backs the idea of a detachment formed in a zone partly in the basement but also in the nappe.

There are several reasons to believe that the NSDZ did not play a part in bringing the units into close proximity of each other. From these analyses it is apparent that the monazites in the basement rock and the nappe rock formed at about the same time during the Finmarkian. Monazites formed at the same time in both units indicates that the units were already in juxtaposition before final obduction. This is also underlined by the gradual transition of metamorphic grade from one unit into the next with distance from the detachment. Furthermore, from the field research it is clear that the NSDZ does not continuously run along the tectostratigraphic contacts but cuts the basement-nappe contact at several occasions.

The last cross section (EF) runs across a basement-nappe contact which is marked by a shear zone. Again the basement mainly consists of gneisses and the nappe consists of schist. The schist in this case accommodated most of the shearing along the shear zone. Close to the basement-nappe contact the schist is heavily crenulated and has large amounts of chlorite. At larger distance from the shear zone the schist consists more and more of biotite and muscovite with towards the end of the cross sections containing even small garnets. This clearly shows that metamorphic conditions change with intensity by which the rock is affected by the movement on the shear zone. On the fault the rock has a mylonitic texture which has large quantities of chlorite. The rock has a few brittle fractures which are again filled with chlorite.

## 5.2 Resetting of the U-Th-Pb system

Sample 22.9 and 22.5 which have been used for geochronology contained relative small monazite grains. Monazites in these rocks are likely to have been affected by forms of mineral break down processes. The grain size of monazites in sample 22.9 is on average slightly smaller than those in 22.5 which could indicate that sample 22.9 was more reworked hence more break down of monazite, or that this sample was undergoing low grade metamorphism for a longer period encouraging more break down of the monazite.

Other evidence of monazite break down are found in two other samples (22.1 and 21.6) from cross section EF where former monazites have left “spaces” in the mineral structure containing large amounts of phosphor and trace elements. Another indicator of secondary processes having affected the monazite minerals are the secondary monazite formations on the edge of apatite grains.

Because of this it is likely that most of the monazites have undergone some resetting of the U-Th-Pb system explaining the low U, Th and Pb contents of most of the monazites. There is several ways of resetting the U-Th-Pb system in monazite. Heating the monazite past the closure temperature can cause Pb and possibly U or Th to diffuse from the monazite. In the upper amphibolite facies and granulite facies monazite becomes an open system with respect to U-Pb because of the increased diffusion of lead (Smith and Giletti, 1997). During cooling the system closes again at the closure temperature at which measurable quantities of radiogenic lead begin to accumulate.

Zhu et al. (1999) showed that secondary lattice replacement/recrystallization is a second process of monazite resetting. The U-Th-Pb system in monazites can be affected by recrystallization, often enhanced by fluids (Cherniak et al., 2004). There are several ways by which monazite can recrystallize; by for example high temperature coarsening of the matrix phase or fluid-mediated recrystallization (Cherniak et al., 2004). Under these latter conditions, monazite is very unstable and can break down at very low temperatures. For this reason it is sometimes difficult to use monazite as geochronometers. However, in this case it is still possible to use them in as markers of the metamorphic environment that they recrystallized/ or formed again in prograde metamorphic reaction.

When monazite-containing rock enters a low-grade metamorphic environment the monazite breaks down to form a range of light rare-earth element (REE)-enriched phosphates (e.g. allanite, xenotime, apatite) (Smith and Barreiro, 1990; Foster et al., 2002). For example, sample 22.5 has recrystallized monazite on the grain boundaries of apatite which means that new monazite was formed possibly by recrystallization of older monazites during retrograde metamorphism. For accessory phases it is energetically favourable to stay on grainboundaries and therefore they will move during recrystallization of monazites through dissolution and precipitation (Cherniak et al., 2004). After nucleation and growth of the monazite the dissolution of apatite is then enhanced along its grainboundary. This then in turn catalyzes the growth of the monazite (Harlov et al., 2002).

### 5.3 Exhumation in the Western Gneiss Region

The results from the study done on the detachment in the Naustdal region fit well with some of the models which were developed for the exhumation in the WGR. It is evident that in the Naustdal region the NSDZ is a  $\geq 2$  kilometer wide zone with top to the west movement. It is also clear that the juxtaposition of the nappe and basement and the formation and localization of the NSDZ have to be considered separately.

Both the nappe and basement in the Naustdal region contain monazites which formed during the Finmarkian orogeny. After their formation the monazites would have been subjected to subduction to possible depths of up to 130 km. It is still debatable if monazites can survive a subduction cycle. The monazite formation can only indicate that both the basement and the nappe already existed before the Scandian as two separate units and secondly that these units were in the same PT conditions (temperature range under which monazites can form) simultaneously.

Displacement along the NSDZ was accommodated in the amphibolite to chlorite facies. Any shearing under deeper conditions is not visible. This supports the two stage exhumation model where the NSDZ was only active during crustal exhumation (Andersen et al., 1994; Terry and Robinson, 2003). However, some of the crustal shear movement was accommodated by shear zones which run sub-parallel to the NSDZ. Even though the NSDZ does not continuously run along the basement-nappe contact and in some places the NSDZ cuts right through the different units, it cannot be excluded that NSDZ played a large role in bring the units in close proximity as it is the only major shear zone still visible today.

The detachment did not only affect the Precambrian basement but also the overlying nappes implying that the detachment had some influence on the thinning of the nappes. However, the extent of this influence was probably only limited as the affect of the NSDZ cannot be observed throughout the whole nappe units.

## 6. Conclusion

In this study a number of issues were addressed with respect to the exhumation of the Western Gneiss Region. The Naustdal region has proven to give an insights which are important to the exhumation at larger scale.

Some of the conclusive points are:

1. Both the basement and nappes are affected by the NSDZ in a up to at least 2 km wide zone which implies that the NSDZ will in some parts have been part in the thinning of the nappes.
2. The NSDZ is not localized entirely on the basement-nappe contact however it can be assumed that because this is the only major detachment in the WGR it must have had some influence on the relative basement-nappe positioning.
3. The NSDZ was active during the amphibolite and chlorite facies and possibly at deeper levels.
4. Monazite growth in both the Precambrian basement and the nappes took place during the Finmarkian orogeny. Apparent ages indicate that the units were at similar metamorphic conditions at ~ 500 Ma.
5. The large variability among the monazites from sample 22.9 and the secondary growth of monazite on apatite is an indication of poly-metamorphism.

The concept of geochronology and the determination of temperature-time path metamorphism have many uncertainties when it is based on the closure temperature of monazite. Monazite is highly likely to be affected by retrograde metamorphism in the form of resetting the system and recrystallization of the monazites in the rock. Furthermore in this research there were problems with the grainsize and with errors on measurements, large spread of apparent ages and inconsistent isochron ages.

## Acknowledgments

Many thanks to Dr. Herman L.M. van Roermund for his help in setting up this research and assisting during the field research in Norway and subsequent work in Utrecht. I would like to thank Valby van Schijndel for being a great field partner and Dr. Dirk Spengler for his help on finding literature and motivating words. Furthermore I would like to thank the Molengraaff Foundation, Delft, the Netherlands, who made this research possible by funding the field trip and the microprobe research. For help with operating the microprobe I also would like to thank Tilly Bouten as she was always there to make sure I was able to do the microprobe analyses.

## References

- Andersen, T.B., Jamtveit, B., 1990. Uplift of deep crust during orogenic extensional collapse: a model based on field studies in the sogn-sunnfjord region of western Norway. *Tectonics*, 231, pp. 1097-1111
- Andersen, T.B., Osmundsen, P.T., Jolivet, L., 1994. Deep crustal fabrics and a model for extensional collapse of the southwest Norwegian Caledonides. *Journal of Struct. Geol.* 16, 1191- 1203
- Andersen, T.B., 1998. Extensional tectonics in the Caledonides of southern Norway, an overview. *Tectonophysics*, 285, pp. 333-351
- Andersen, T., B., Berry, H.N., Lux, D.R., Andresen, A., 1998. The tectonic significance of pre-Scandian Ar-Ar phengite cooling ages in the Caledonides of western Norway. *J. Geol. Soc.*, 155, pp. 297-309
- Andersen, T.B., Austrheim, H., 2003. Norway eclogite symposium, Pre-symposium excursion: Bergen – Selje, *Physics Geological Processes*, pp. 70
- Bingen, B., Van Breemen, O., 1998. U-Pb monazite ages in amphibolite- to granulite-facies orthogneiss reflect hydrous mineral breakdown reactions: Sveconorwegian Province of SW Norway. *Contrib. Mineral Petrol.* 132, pp. 336-353
- Bockelie, J.F., Nystuen, J.P., 1985. The southern eastern part of the Scandinavian Caledonides. In: *The Caledonide Orogeny – Scandinavia and Related areas* (eds. Gee, D.G. and Sturt, B.A.) pp 69-88. Chichester: John Wiley & Sons
- Braathen, A., 1999. Kinematics of post-Caledonian polyphase brittle faulting in the Sunnfjord region, western Norway, *Tectonoph.*, 302, pp. 99-121
- Brueckner, H., K., Roermund, H., L., M., 2004. Dunk Tectonics: a multiple subduction/duction model for the evolution of the Scandinavian Caledonides. *Tectonics*, 23 pp. 1-20
- Bryhni, I., Sturt, B.A., 1985. Caledonides of southern Norway. In: *The Caledonide Orogen-Scandinavia and related areas* (eds. Gee, D.G., Sturt, B.A.), John Wiley, Chichester, pp. 89-107
- Bryhni, I., Lytro, O., 2000. Berggrunnskart Naustdal 1218 III, M 1:(50000). Forelopig utgave Norges Geologiske Undersokelse
- Carswell, D.A., Brueckner, H.K., Cuthbert, S.J., Mehta, K., O'Brien, P.J., 2003. The timing of stabilization and the exhumation rate for ultra-high pressure rocks in the western gneiss region Norway, *J. Metam. Geol.*, 21, pp. 601-612

- Chauvet, A., Dallmeyer, R.D., 1992.  $^{40}\text{Ar}/^{39}\text{Ar}$  mineral dates related to Devonian extension in the southwestern Scandinavian Caledonides. *Tectonophys.* 210, pp. 155-177
- Cherniak, D.J., Watson, E.B., Grove, M., Harrison, T.M., 2004. Pb diffusion in monazite: A combined RBS/SIMS study. *Geoch. Cosmochim. Acta*, 68, pp. 829-840
- Cocks, L.R.M., and Torsvik, T.H., 2002. Earth History 500 – 400 Ma: a faunal and palaeomagnetic review, *J. Geol. Soc. Lon.*, 159, pp. 631 - 644
- Corfu, F., Andersen, T.B., 2002. U-Pb ages of the Dalssjøfjord Complex, SW Norway, and their bearing on the correlation of allochthonous crystalline segments of the Scandinavian Caledonides. *Int. J. of Earth Sci.* 91, pp. 955-963
- Dallmeyer, R.D., Stephens M.B., 1991. Chronology of eclogite retrogression within the Seve Nappe Complex, Råvvaure, Sweden: evidence from  $^{40}\text{Ar}/^{39}\text{Ar}$  mineral ages. *Geol. Rundsch.*, 80, pp. 729-743
- Dewey, J.F., 1993. Transtension in Arcs and Orogens. *Int. Geol. Rev.* 44, pp. 402-439
- Dewey, J.F., Ryan, P.D., Andersen, T.B., Orogenic uplift and collapse, crustal thickness, fabrics and metamorphic phase changes: the role of eclogites. From Prichard, H. M., Alabaster, T., Harris, N. B. W. & Neary, C. R. (eds), 1993, *Magmatic Processes and Plate Tectonics*, *Geol. Soc. Special Publ.* 76, 325-343
- Dodson, M.H., 1973. Closure temperature in cooling geochronological and petrological systems. *Contr. Min. Petrol.* 40 pp. 259-274
- Dobrzhinetskaya, L.F., Eide, E.A., Larsen, F.B., Sturt, B.A., Tronnes, R.G., Smith, D.C., Taylor, W.R., Posukhova, T.B., 1995. Microdiamonds in high-grade metamorphic rocks of the Western Gneiss Region, Norway, *Geology*, 23, pp. 597-600
- Ellis, D.J., Geen, D.H. (1979). An experimental study of the effect of Ca upon garnet-clinopyroxene Fe-Mg exchange equilibria. *Contrib. Mineral. Petrol.* 71, 13-22.
- Fossen, H., 1992. The role of extensional tectonics in the Caledonides of south Norway. *J. Struc. Geol.*, 14, pp. 1033-1046
- Fossen, H., Dunlap, W.J., 1998. Timing and kinematics of Caledonian thrusting and extensional collapse, southern Norway: evidence from  $^{40}\text{Ar}/^{39}\text{Ar}$  thermochronology. *J. of Struct. Geo.* 20, pp. 765-781.
- Foster, G., Kinny, P., Vance, D., Prince, C., Harris, N., 2000. The significance of monazite U-Th-Pb age data in metamorphic assemblages; a combined study of monazite and garnet chronometry. *Earth Plan. Sci. Let.* 181, pp. 327-340
- Foster, G., Gibson, H.D., Parrish, R., Horstwood, M., Fraser, J., Tindle, A., 2002. Textural, chemical and isotopic insights into the nature and behaviour of metamorphic monazite. *Chem. Geol.*, 191, pp. 183-207
- Gibson, H.D., Carr, S.D., Brown, R.L., Hamilton, M.A., 2004. Correlations between chemical and age domains in monazite, and metamorphic reactions involving major pelitic phases: an integration of ID-TIMS and SHRIMP geochronology with Y-Th-U X-ray mapping. *Chem. Geol.* 211, pp. 237-260
- Giles, D., Nutman, A.P., 2002. SHRIMP U-Pb monazite dating of 1600-1580 Ma amphibolite facies metamorphism in the southeastern Mt Isa Block, Australia. *Aust. Journal of Earth Sci.* 49, 455-465
- Griffin, W.L., Brueckner, H.K. (1985). REE, Rb-Sr and Sm-Nd studies of Norwegian Eclogites. *Chem. Geol.* 52, 249-271
- Hacker, B.R., Andersen, T.B., Root, D.B., Mehl, L., Mattinson, J.M., Wooden, J.L., 2003. Exhumation of high-pressure rocks beneath the Solund Basin, Western Gneiss Region of Norway. *J. metamorphic Geol.* 21, pp. 613-629

- Harings, M., 2005. Monazite EMP geochronology, applied to a multistage metamorphic terrane: The broken Hill Block, New South Wales, Australia, Utrecht University
- Harlov, D.E., Foester, H.-J., Nijland, T.G., 2002. Fluid-induced nucleation of (Y + REE)-phosphate minerals within apatite: Nature and experiment. Part I. Chlorapatite. *Am. Mineral.* 87, pp. 245-261
- Hossak, J.R., 1984. The geometry of listric normal faults in the Devonian basins of Sunnfjord, W. Norway. *J. Geol. Soc. Lon.*, 141, pp. 629-637
- Johnston, S.M., Hacker, B.R., Andersen, T.B., 2007. Exhuming Norwegian ultrahigh-pressure rocks: Overprinting extensional structures and the role of the Nordfjord-Sogn Detachment Zone. *Tectonics*, 26, pp. 1-12
- Krabbendam, M., Dewey, F., 1998. Exhumation of the UHP rocks by transtension in the Western Gneiss Region, Scandinavian Caledonides. *Geol. Soc. Spec. Publ.* 135 pp. 159-181
- Labrousse, L., Jolivet, L., Andersen, T.B., Agard, P., Maluski, H., Schaerer, U., 2004. Pressure-temperature-time deformation history of the exhumation of ultra-high pressure rocks in the western Gneiss Region, Norway. *Geol. Soc. Am. Spec. Paper*, 380, pp. 155-185
- Marques, F.O., Schmid, D.W., Andersen, T.B., 2007. Applications of inclusion behaviour models to shear zone system: The Nordfjord-Sogn Detachment Zone in western Norway. *J. Struc. Geol.* 29, pp. 1622-1631
- McKerrow, W.S., Niocail, C.M., Dewey, J.F., 2000. The Caledonian orogeny redefined. *J. of Geol. Soc.* 157, pp. 1149-1154.
- Nagy, G., Draganits, E., Demeny, A., Panto, G., Arkai, P., 2002. Genesis and transformations of monazite, florencite and rhabdophane during medium grade metamorphism: examples from the Sopron Hills, Eastern Alps. *Chem. Geol.* 191, pp. 25-46
- Nriagu, J.O., Moore, P.B., 1984. Phosphate minerals, Springer-Verlag Berlin Heidelberg New York, 1984
- Osmundsen, P.T., Andersen, T.B., 2001. The middle Devonian basins of Western Norway: sedimentary responds to transtensional tectonics? *Tectonophys.* 332, pp. 51-86
- Parrish, R.R., 1990. U-Pb dating of monazite and its application to geological problems. *Can. J. Earth Sci.*, 27, pp. 1431-1450
- Smith, D.C., 1984. Coestie in clinopyroxene in the Caledonides and its implications for geodynamics, *Nature*, 310, pp. 641-644
- Smith, H.A., Barreiro, B., 1990. Monazite U-Pb dating of staurolite grade metamorphism in pelitic schists. *Cont. to Mineralogy and Petrology* 105, 602-615
- Smith, H.A., Giletti, B.J., 1997. Lead diffusion in monazite. *Geochemica et Cosmochimica Acta* 61, 1047-1055
- Roberts, D., Gee, D.G., 1985. An Introduction to the structure of the Scandinavian Caledonides. In: *The Caledonide Orogen- Scandinavia and Related Areas* (eds. Gee, D.G., Sturt, B.A.), pp. 55-68, John Wiley, Chichester
- Roberts, D., 2003. The Scandinavian Caledonides: event chronology, palaeo-Geographic settings and likely modern analogues, *Tectonoph.*, 365, 283-299

- Terry, M.P., Robinson, P., Hamilton, M., Jercinovic, M.J., 2000. Monazite geochronology of UHP and HP metamorphism, deformation, and exhumation, Nordoyane, Western Gneiss Region, Norway. *Am. Min.* 85, pp. 1651-1664
- Terry, M., P., Robinson, P., 2003. Geometry of eclogite-facies structural features: Implications for production and exhumation of ultra-high pressure rocks, Western Gneiss Region, Norway. *Tectonics*, 23, pp. 1-23
- Teufel, S., Heinrich, W., 1997. Partial resetting of the U-Pb isotope system in monazite through hydrothermal experiments: An SEM and U-Pb isotope study. *Chem. Geol.* 137 pp. 273-281
- Torsvik, T.H., Smethurst, M., Meert, J., Van der Voo, R., McKerrow, W.S., Brazier, M., Sturt, B.A., and Walderhaug, H., 1996. Continental break-up and collision in the Neo-proterozoic and Palaeozoic – a tale of Baltica and Laurentia, *Earth-Sci. Rev.*, 40, pp. 229 - 258
- Torsvik, T.H., 1998. Palaeozoic palaeogeography: A North Atlantic viewpoint, *GFF*, 120, pp. 109 -118
- Van Roermund, H.L.M., Drury, M.R., 1998. Ultra-high pressure ( $P > 6$  GPa) garnet peridotites in Western Norway: exhumation of mantle rocks from  $> 185$  km depth. *Terra Nova*, 10, pp. 295-301
- Van Roermund, H.L.M., Carswell, D.A., Drury, M.R., Heijboer, T.C., 2002. Microdiamonds in a megacrystic garnet websterite pod from Bardane on the island of Fjærtoft, western Norway: Evidence for diamond formation in mantle rocks during deep continental subduction. *Geol. Soc. Am.* 30, pp. 959-962
- Van Roermund, H.L.M., 2007. Recent progress in the northernmost UHPM domain of the Western Gneiss Region, Norway: Scandian subduction down to 180-200 km depths. Abstract International Eclogite Field Symposium 2007
- Wing, B.A., Ferry, J.M., Harrison, T.M., 1993. Prograde destruction and formation of monazite on the electron microprobe: Deconvoluting multistage tectonic histories. *Geology*, 27, pp. 1023-1026
- Zhu, X.K., O’Nions, R.K., 1999. Zonation of monazite in metamorphic rocks and its implications for high temperature thermochronology: a case study from the Lewisian terrain. *Earth Planet. Sci. Lett.* 171, pp. 209-220

